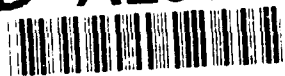
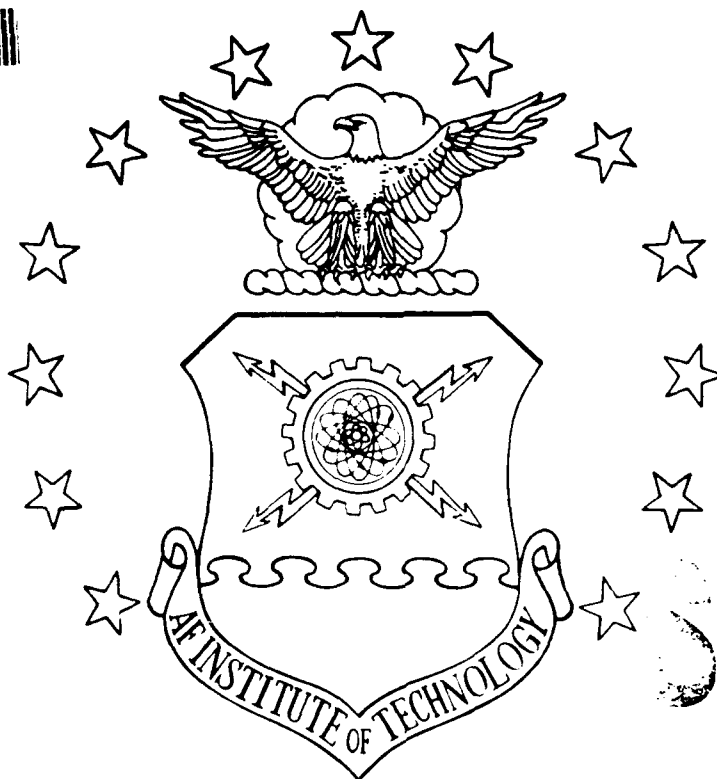


AD-A256 438



1



OCT 27 1992

E

D

WING ROCK PREDICTION METHOD  
FOR A HIGH PERFORMANCE  
FIGHTER AIRCRAFT

THESIS

Robert C. Nolan II  
Captain, USAF

AFIT/GAE/ENY/92J-02

DEPARTMENT OF THE AIR FORCE  
AIR UNIVERSITY

**AIR FORCE INSTITUTE OF TECHNOLOGY**

Wright-Patterson Air Force Base, Ohio

DISTRIBUTION STATEMENT A

Approved for public release  
Distribution Unlimited

①

AFIT/GAE/ENY/92J-02

**WING ROCK PREDICTION METHOD  
FOR A HIGH PERFORMANCE  
FIGHTER AIRCRAFT**

**THESIS**

**Robert C. Nolan II  
Captain, USAF**

**AFIT/GAE/ENY/92J-02**

**Approved for public release; distribution unlimited**

**92-28247**  


**WING ROCK PREDICTION METHOD FOR A HIGH-PERFORMANCE  
FIGHTER AIRCRAFT**

**THE SIS**

**Presented to the Faculty of the School of Engineering  
of the Air Force Institute of Technology**

**Air University**

**In Partial Fulfillment of the  
Requirements for the Degree of  
Master of Science in Aeronautical Engineering**

**Robert C. Nolan II, B.S.**

**Captain, USAF**

**May 1992**

Approved for	
DIST. G-14	
By	
E. C. 1	
Approved for	
Dist	Approved for
A-1	

## Preface

The purpose of this study was increase the body of knowledge concerning the unstable roll oscillations known as wing rock. The basic stability mode and the critical stability derivatives which contribute to this motion were identified. A simple procedure to predict wing rock motion in swept wing fighter designs was developed. Finally, a flight test was flown to confirm the analytical findings of this study.

I would like to thank those people who helped me complete this work, especially Dr. Brad Liebst, my AFIT advisor, and Major Dan Gleason, the AFIT/TPS liaison.

Robert C. Nolan II

## Table of Contents

	Page
Preface . . . . .	ii
List of Figures . . . . .	vi
List of Tables . . . . .	viii
List of Symbols . . . . .	ix
Abstract . . . . .	xiii
 I. Introduction . . . . .	 1-1
Background . . . . .	1-1
Objectives . . . . .	1-3
Methods . . . . .	1-4
Limitations . . . . .	1-5
 II. Analysis Techniques, Aircraft Descriptions and Equations of Motion . . . . .	 2-1
Small-Perturbation Theory . . . . .	2-1
Typical Modes of Motion of a Dynamically Stable Aircraft . . . . .	 2-3
Longitudinal Motion . . . . .	2-3
Lateral Directional Motion . . . . .	2-5
Bifurcation Analysis . . . . .	2-7
Equilibrium and Stability . . . . .	2-8
Limit Cycles . . . . .	2-11
Bifurcation Diagrams and Parameters . . . . .	2-14
Limit points . . . . .	2-15
Hopf Bifurcations . . . . .	2-16
Bifurcation Software . . . . .	2-17
Program Capabilities . . . . .	2-18
Methods . . . . .	2-19
Aircraft Description . . . . .	2-21
McDonnell Douglas F-15 Eagle . . . . .	2-21
McDonnell Douglas F-4 Phantom . . . . .	2-22
Northrop T-38 Talon . . . . .	2-23

Basic Aircraft Model . . . . .	2-24
Aircraft Equations of Motion . . . . .	2-24
Aerodynamic Force and Moment Coefficients . . . . .	2-32
Starting Point Selection . . . . .	2-34
III. Analytical Results . . . . .	3-1
Bifurcation Analysis . . . . .	3-1
Eigenvalue Analysis . . . . .	3-5
Linearization Around the Trigger Point . . . . .	3-10
Eigenvector Analysis . . . . .	3-12
Characteristic Equation . . . . .	3-14
Validation of Expression . . . . .	3-18
Prediction Procedure . . . . .	3-20
Critical Stability Derivatives . . . . .	3-22
IV. Application of Analytical Results . . . . .	4-1
V. Flight Test Method . . . . .	5-1
Test Item Description . . . . .	5-1
Data Reduction . . . . .	5-3
Test Conditions and Methods . . . . .	5-4
VI. Flight Test Results . . . . .	6-1
T-38A Flight Test Results . . . . .	6-1
Data Analysis . . . . .	6-1
T-38 Test Crew Comments . . . . .	6-9
RF-4C Flight Test Results . . . . .	6-10
Data Analysis . . . . .	6-10
RF-4C Test Crew Comments . . . . .	6-14
VII. Conclusions and Recommendations . . . . .	7-1
Conclusions . . . . .	7-1
Recommendations . . . . .	7-4
Appendix A: McDonnell Douglas F-15 Physical Data . . . . .	A-1
Appendix B: McDonnell Douglas F-4 Physical Data . . . . .	B-1
Appendix C: Northrop T-38 Physical Data . . . . .	C-1
Appendix D: Fighter Inertia Characteristics . . . . .	D-1
Appendix E: RF-4C/T-38A DAS Parameters . . . . .	E-1

Bibliography . . . . . F-1

Vita . . . . . G-1

## List of Figures

	Page
Figure 2.1 Short Period Mode . . . . .	2-3
Figure 2.2 Phugoid Mode . . . . .	2-4
Figure 2.3 Spiral Mode . . . . .	2-6
Figure 2.4 Dutch Roll Mode . . . . .	2-7
Figure 2.5 Van der Pol Trajectory . . . . .	2-12
Figure 2.6 Wing Rock Limit Cycle . . . . .	2-13
Figure 2.7 Bifurcation Diagram With Limit Point . . . . .	2-15
Figure 2.8 Diagram with a Hopf Bifurcation . . . . .	2-17
Figure 2.9 Aircraft Body Axes . . . . .	2-26
Figure 2.10 Gravity Vector and Body Axes . . . . .	2-27
Figure 2.11 Aircraft Velocity Components . . . . .	2-28
Figure 3.1 Alpha Bifurcation Diagram for F-15 . . . . .	3-2
Figure 3.2 Beta Bifurcation Diagram for F-15 . . . . .	3-3
Figure 3.3 F-15 Flight Test Results . . . . .	3-4
Figure 3.4 Eigenvalues at $\text{Alpha} = 10^\circ$ for F-15 . . . . .	3-5
Figure 3.5 Root Locus for F-15 Varying Alpha . . . . .	3-8
Figure 3.6 Dutch Roll and Roll Modes for F-15 . . . . .	3-9
Figure 3.7 Dutch Roll and Spiral Modes for F-15 . . . . .	3-9
Figure 3.8 Magnitude of Eigenvectors at Trigger Point for F-15 . . . . .	3-13

Figure 3.9	Fighter Mass Distribution	3-15
Figure 3.10	Wing Rock Parameter vs Alpha for F-15	3-20
Figure 4.1	AOA vs Trigger Parameter for F-4J	4-2
Figure 4.2	F-4 Trimmed Lift Curve	4-3
Figure 6.1	T-38A Wing Rock Prediction	6-3
Figure 6.2	AOA vs Time From Wing Rock Onset	6-5
Figure 6.3	Roll Angle 1 second After Onset	6-5
Figure 6.4	Roll Angle vs Time From Onset	6-6
Figure 6.5	Roll Angle and Alpha vs Time T-38A	6-6
Figure 6.6	T-38A Wing Rock Limit Cycle	6-8
Figure 6.7	RF-4C Wing Rock Prediction	6-10
Figure 6.8	Angle of Attack vs Time From Wing Rock Onset	6-12
Figure 6.9	Roll Angle Magnitude Following Wing Rock Onset	6-13
Figure 6.10	RF-4C Wing Rock Limit Cycle	6-14

## List of Tables

	Page
Table 3.1 State Variables at Hopf Point for F-15 . . . . .	3-4
Table 3.2 Longitudinal Mode Characteristics for F-15 . . . . .	3-6
Table 3.3 Lateral Mode Characteristics for F-15 . . . . .	3-6
Table 3.4 Eigenvalues at $\alpha$ equal 10,21,30 degrees for F-15 . . . . .	3-7
Table 3.5 Wing Rock Parameter and Coefficient Values for F-15 . . . . .	3-19
Table 4.1 Trigger Parameter and Coefficient values for F-4J . . . . .	4-1
Table 5.1 Test Parameters . . . . .	5-4
Table 5.2 Test Point Summary . . . . .	5-6
Table 6.1 Predicted Trigger Parameter Values T-38A . . . . .	6-2
Table 6.2 Summary of T-38 Flight Test Results . . . . .	6-4
Table 6.3 Summary of RF-4C Flight Test Results . . . . .	6-11

### List of Symbols

$\alpha$	: angle of attack (degrees)
$\beta$	: sideslip angle (degrees)
$\delta_a$	: aileron deflection angle (degrees)
$\delta_{dt}$	: differential tail deflection angle (degrees)
$\delta_e$	: elevator (stabilator) deflection angle (degrees)
$\delta_r$	: rudder deflection angle (degrees)
$\zeta$	: damping ratio
$\lambda$	: eigenvalue
$\phi$	: roll angle (degrees)
$\Theta$	: pitch angle (degrees)
$\omega$	: frequency (cycles/second)
$a_x$	: forward acceleration
$b$	: wing span (feet)
$C_D$	: drag coefficient
$C_L$	: lift coefficient
$C_l$	: rolling moment coefficient
$C_{lw}$	: Rolling moment due to sideslip
$C_{lp}$	: roll damping
$C_M$	: pitching moment coefficient
$C_N$	: yawing moment coefficient

$C_{n\beta}$  : yawing moment due to sideslip  
 $C_{Np}$  : yawing moment due to roll rate  
 $C_{Nr}$  : yaw damping  
 $C_X$  : x axis force coefficient  
 $C_Y$  : y axis force coefficient  
 $C_{Y\beta}$  : side force due to sideslip  
 $C_{Yp}$  : side force due to roll rate  
 $C_{Yr}$  : side force due to yaw rate  
 $C_Z$  : z axis force coefficient  
 $c$  : control vector  
 $c_i$  : single parameter used in continuation  
 $c_0$  : critical parameter value  
 $C$  : mean aerodynamic chord (feet)  
 $f$  : vector function  
 $f_i$  : function describing dynamics of state  $i$   
 $f_u$  : Jacobian matrix  
 $f_c$  : matrix of partial derivatives  
 $g$  : gravitational constant (32.2 ft/sec<sup>2</sup>)  
 $h$  : local deviation form of  $f$   
 $h_i$  : local deviation form of  $f_i$   
 $i$  : sqrt -1  
 $I_x$  : moment of inertia about the x axis

$I_{xz}$  : cross product of inertia in the x-z plane  
 $I_y$  : moment of inertia about the y axis  
 $I_z$  : moment of inertia about the z axis  
 $L$  : rolling moment  
 $M$  : pitching moment  
 $M$  : monodromy matrix  
 $m$  : aircraft mass  
 $N$  : yawing moment  
 $p$  : roll rate (rads/sec)  
 $Q$  : dynamic pressure (lbf/ft<sup>2</sup>)  
 $q$  : pitch rate (rads/sec)  
 $r$  : yaw rate (rads/sec); also, amplitude of limit cycle  
 $S$  : wing planform area (ft<sup>2</sup>)  
 $s$  : arclength; also LaPlace variable  
 $T$  : thrust force; also limit cycle period  
 $T_{1/2}$  : time to half amplitude  
 $T_2$  : time to double amplitude  
 $t$  : time  
 $u$  : vector of model states  
 $u_i$  : model state  $i$   
 $u$  : aircraft speed in the x axis direction  
 $V_{tr}$  : true aircraft speed

$v$  : aircraft speed in the y axis direction

$w$  : aircraft speed in the z axis direction

$X$  : force in the x axis direction

$X\phi$  : trigger parameter

$y$  : Distance of center of pressure from leading edge (ft)

$Y$  : force in the y axis direction

$Z$  : force in the z axis direction

Abstract

This study is a limited investigation of the nonlinear aircraft behavior known as wing rock.

An eight state F-15 model is analyzed using bifurcation theory and equilibrium and limit cycle solutions to the nonlinear equations of motion are computed. The wing rock onset point is identified and small perturbation analysis is used to linearize the equations of motion about this point. The eigenstructure of the model is analyzed and is used to identify the stability modes involved in this motion. A procedure is developed to predict wing rock onset and frequency and the critical stability derivatives involved in this behavior are identified. The developed procedure is applied to existing F-4J data and a flight test involving RF-4C and T-38A aircraft is flown.

The results show wing rock is an unstable dutch roll motion and the developed wing rock prediction parameter is accurate to within  $1^\circ$  of onset AOA. The frequency prediction parameter gives a fair estimate of wing rock motion but it may be adversely influenced by the type of flight test data. The slope of the prediction parameter versus AOA curve may be an indication of wing rock magnitude and frequency.

# WING ROCK PREDICTION METHOD FOR A HIGH PERFORMANCE FIGHTER AIRCRAFT

## I. Introduction

### Background

Many modern day combat aircraft exhibit lightly damped rolling oscillations at moderate to high angles-of-attack. These motions are commonly referred to as wing rock. Wing rock can have a wide ranging effect on an aircraft's ability to complete its mission. Wing rock may present itself as a minor nuisance during noncritical maneuvering or as a major headache while trying to track an enemy target. For some configurations wing rock is an early warning of impending departure or spin entry (19:1). In some aircraft the severity of wing rock could create sufficient inertial and kinematic coupling to cause angle-of-attack excursions leading to loss of control. This problem may present itself during the landing phase as well as during maneuvering flight.

Two different types of wing rock have been identified by previous research (19:1). The first is characterized by unsteady lateral motions at moderate to high angles-of-attack. These motions exhibit small-amplitude intermittent roll oscillations and maybe a function of pilot vehicle interaction. Here the roll motion is not periodic. This type of wing rock is normally associated with low airspeed, high angle-of-attack (AOA) flight in gusty conditions such as during approach and landing. The second type of wing rock is manifested as an initially diverging oscillation which becomes periodic in nature and

is generated by a limit cycle mechanism. This motion is characterized by very large changes in roll angle. The second form of wing rock is normally associated with high AOA maneuvering such as in close-in air-combat. Flight procedures can normally be changed to avoid the first type of wing rock without greatly effecting mission accomplishment but the same cannot be said about type 2. If a combat aircraft is not able to track a target due to wing rock it becomes obvious that mission accomplishment has been degraded significantly. This study deals with the second type of wing rock.

The mechanisms which cause wing rock are not fully understood. It appears that wing rock is triggered by some type of flow asymmetry, developed by negative roll damping and then sustained by some type of nonlinear aerodynamic roll damping (10:921). Therefore, aerodynamically wing rock may be caused by flow separation at low speeds or shock-induced separations at transonic speeds, oscillatory aerodynamic loads produced by aircraft motion, or vortex flow dynamics over the wing and fuselage (21:10-2). From the stability point of view it is postulated that wing rock is associated with a sign change in  $C_{nr}$ , reduced roll damping, or instability of one or more of the aircraft's longitudinal and/or lateral control modes. Today's modern fighter aircraft attempt to exploit the maximum lift and agility available by operating at ever increasing angles-of-attack therefore, wing rock will continue to degrade fighter performance. Since it is not currently possible to maintain attached flow at the excessive angles-of-attack required for maneuvering, the wing rock phenomenon is not likely to be attenuated by aerodynamic design alone (19:1). Some type of control system augmentation will probably be necessary to suppress wing rock behavior.

Previous studies have already developed several parameters which provide indications of aircraft behavior at high angles-of-attack. Most notably are the lateral control divergence parameter (LCDP) and  $C_{n\beta, \text{dynamic}}$  or some combination of the two (19). These parameters have been used to predict aircraft departure sensitivity and general departure characteristics. These parameters provide general estimates of aircraft behavior at high AOA. They are not able to specifically predict aircraft motion at high angles-of attack. Both of these parameters were developed for MIL-F-8785C and have been carried forward in MIL-STD-1797A. This study will attempt to take another step forward and develop a parameter that specifically predicts a high AOA behavioral aircraft flight characteristic. This study will look at an aircraft's longitudinal and/or lateral stability modes and examine their effect or contribution to the wing rock phenomenon. An attempt will be made to examine this behavior with the goal of developing a method to predict wing rock onset that is not necessarily aircraft specific. Hopefully, this study will increase the understanding of wing rock and thus help provide better high angle-of-attack handling qualities for fighter aircraft.

## Objectives

The overall objective of this study is to gain critical knowledge of the wing rock phenomenon which will eventually lead to improved aircraft handling qualities. The objective will be accomplished through a detailed examination of the stability modes of a conventional aircraft design (dynamically stable without a flight control system) as the

aircraft begins to wing rock. From this examination an attempt will be made to develop a parameter which will predict wing rock and the frequency of this motion. Once this parameter has been found, a procedure will be developed which will allow an aircraft designer, given certain stability derivatives and inertia characteristics, to predict the onset of wing rock in his design without using complicated software and costly computer time. This study will also attempt to identify the relative importance of the various stability derivatives which contribute to wing rock. Finally, a flight test will be flown to verify the study's results.

The specific objectives of this project are:

1. To examine the longitudinal and lateral stability modes of an aircraft as wing rock begins.
2. Identify the longitudinal and/or lateral modes which contribute to wing rock motion.
3. Develop a parameter which will predict the onset and frequency of wing rock.
4. Develop a procedure an aircraft designer can use to predict wing rock in his design given certain aircraft data, pencil and a pocket calculator.
5. Identify the aircraft stability derivatives critical to the development of wing rock.
6. Conduct a flight test to verify the results of this study.

## Methods

The procedure used to accomplish the objectives presented above follows:

1. Using AUTO-Bifurcation software aircraft data was collected for an elevator sweep to determine the point at which wing rock begins and the state variables at this point.

2. Eigenvalue and eigenvector data was then gathered for each critical point. The eigenvalue data was then used to identify the critical stability modes of the aircraft.
3. Small-perturbation theory was then used to linearize the equations of motion around the wing rock starting point.
4. Eigenvector data was used to eliminate unnecessary states from the aircraft model.
5. From the remaining state matrix's characteristic equation a parameter was developed to predict wing rock motion and its frequency.
6. Given an aircraft's stability and inertia characteristics a relatively simple procedure was developed to predict wing rock.
7. The developed wing rock parameter was then examined to identify which aircraft stability derivatives contribute the most to wing rock.
8. A flight test using the T-38A was flown to confirm the analytical results of this study.

## Limitations

The limitations inherent in this study are mostly related to the flight data for the F-15 model used in the study's analytical portion and the pull-up test maneuver *flown* by the aircraft during both computer simulation and flight test. The data used assumes a flight mach number equal to .6 so this study is only accurate for incompressible mach numbers. The elevator sweep which produced the pull-up maneuver was used in an attempt to decouple the complicated nonlinear equations of motion. Thus this example results in an analysis of pure longitudinal and lateral motion. The pull-up maneuver chosen is not unrealistic as it closely approximates a close-in slow speed scissors or an interceptor's fly-up maneuver to shoot a missile at a high flying target.

## II. Analysis Techniques, Aircraft Descriptions And Equations of Motion

In this section analysis techniques used in this study are discussed, the aircraft used are presented and the model equations of motion are developed. Specifically, this section will review small-disturbance theory, longitudinal and lateral natural motion and bifurcation theory. Following the theory review, the McDonnell-Douglas F-15 Eagle, F-4 Phantom and the Northrop T-38 Talon are introduced. Finally, the development of the aircraft mathematical model and the vehicle equations of motion are discussed.

### Small-Perturbation Theory

The nonlinear equations of motion used in this study are linearized using small-disturbance theory. These equations are linearized about the point at which wing rock begins during the elevator sweep. The resulting linear expressions will then be used in conjunction with eigenvector data in an attempt to parameterize wing rock motion. Small-disturbance theory is normally applied to problems in which small-amplitude motions are present. The aircraft in this study are undergoing some large amplitude motions so the standard linearization process was modified to take this motion into account. Following is a brief description of small-disturbance theory and the linearization process. The following references were used in preparing this section (17:92-95;16:233-239).

Small-disturbance theory is based on the premise that the total motion of an aircraft consists of two parts: a baseline motion that is representative of the operating point or the trim condition and a dynamic motion that accounts for small deviations about the baseline motion. An example would be a wind gust that causes a 1 degree pitch up from unaccelerated wings level flight. Here the small pitch up is the deviation and unaccelerated wings level flight is the baseline condition. Using this concept all the state variables in the equations of motion are replaced by a baseline value plus a disturbance. Thus as per our example pitch would be represented as  $\theta_0 + \delta\theta$  where  $\theta_0$  is the baseline value and  $\delta\theta$  is the pitch disturbance. A function of a state variable may be represented as the first two terms of its Taylor Series expansion. Once the baseline and disturbance variables are substituted into the equations of motion the equations are expanded and the baseline motion is subtracted to leave the perturbed equations. Within the perturbed expressions the products and squares of the disturbance variables are considered negligible in comparison with the disturbance conditions and are thus eliminated. The same is true of the higher order terms of the Taylor Series expansion of a function. Normally, the small-angle assumption (the disturbances and the baseline angles are assumed to be small enough so that the sines of these angles are approximately the angles themselves and the cosines are equal to one) is also made to further simplify the perturbed equations of motion. In this study some of the baseline angles are fairly large so the small angle assumption will not be made and the sines and cosines will take on their actual values.

## Typical Modes of Motion a Dynamically Stable Aircraft

Dynamically stable aircraft have been found to exhibit definite modes of motion. These modes represent natural aircraft motions. As stated earlier, this study will attempt to identify the mode or modes which contribute to wing rock motion. This section will describe these modes.

Longitudinal Motion. The principle longitudinal state variables are velocity, angle-of-attack, and pitch. Aircraft longitudinal motion consists of two basic modes.

The first mode consists of a motion that is characterized by a high frequency oscillation. This motion is often heavily damped and thus subsides quickly. This mode is usually referred to as the *short period mode*. This motion involves rapid changes in angle-of-attack and pitch but the velocity remains essentially constant. The short period mode is illustrated in the following figure.

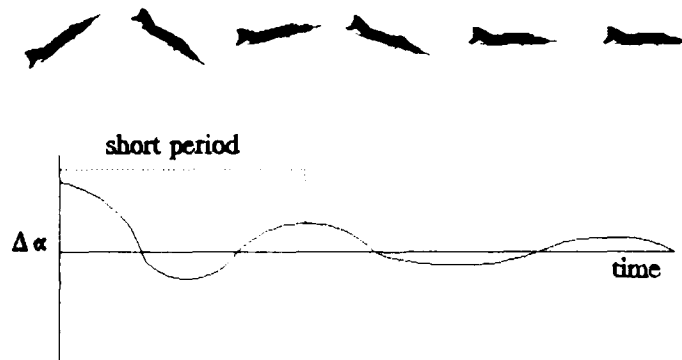


Figure 2.1. Short Period Mode

For a stable short period mode the frequency and damping are normally high thus it is a short lived motion. The short period can be very dangerous if unstable because the pilot cannot correct rapidly enough to prevent a large increase in the motion. This motion is also critical even when stable because the period of oscillation may match the normal pilot response time, approximately 1 or 2 seconds (17:140). There is the possibility that an attempt to forcibly damp an oscillation may actually reinforce the problem and produce an unstable motion (pilot induced oscillation).

The second mode exhibits different characteristics. It consists of variations in velocity and pitch while angle-of-attack remains essentially constant. This mode, normally referred to as the *phugoid mode*, is usually oscillatory and of low frequency.

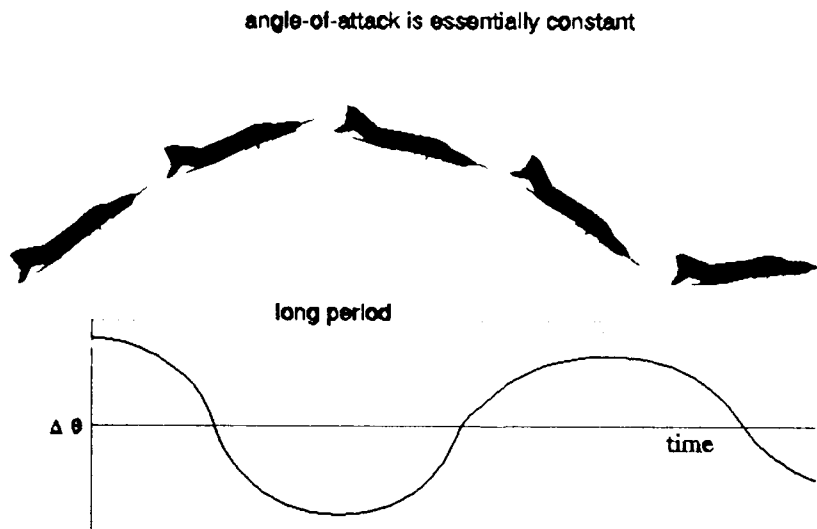


Figure 2.2. Phugoid Mode

Figure 2.2 illustrates the phugoid mode. This motion is normally lightly damped. The phugoid mode is basically a trade of kinetic and potential energy. Pitch and velocity change as the altitude varies. Pilots are often able to tolerate an unstable phugoid. Pilots usually have ample time to counteract the oscillatory nature with very slight control movements due to the motion's long period. For the stable case, the necessary corrections are so small that the pilot may be completely unaware of the aircraft's motion. Both the short period mode and the phugoid mode are characterized by frequency, damping ratio and time to damp (grow) to half (double) amplitude. If the aircraft is modeled as a system of first order differential equations these modes are both represented by a complex conjugate pair of eigenvalues which are the roots of the longitudinal characteristic equation. Note that during phugoid motion the aircraft flight path varies while in the short period mode the aircraft essentially moves in the same direction while pitching about the x wind axis.

Lateral-Directional Motion. The lateral and directional modes are coupled because sideslip ( $\beta$ ) generates both yawing and rolling moments. Therefore coupling exists between roll rate ( $p$ ) and yaw rate ( $r$ ).

The first mode of motion out of the plane of symmetry is called the *spiral mode*. The spiral mode is nonoscillatory and is initiated by a displacement in roll angle. The resulting motion is either stable or unstable. After a roll angle is established if the aircraft returns to wings level flight the motion is stable. If the mode is unstable the aircraft continues to roll and will enter an ever tightening spiral dive and eventually

impact the earth if no correction is made. Like the phugoid mode most pilots tolerate an unstable spiral mode. If the spiral motion is gradual, the pilot can return the aircraft to wings level flight without difficulty.

Figure 2.3 shows the modes characteristics.

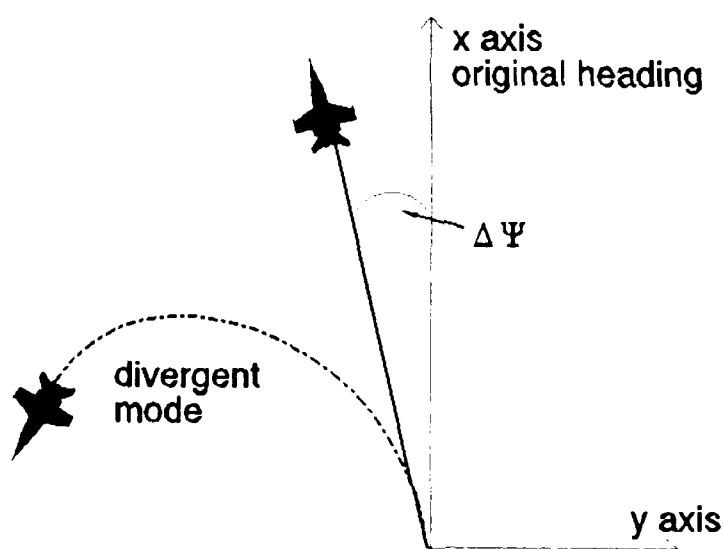


Figure 2.3. Spiral Mode

The next mode is called the *roll mode*. Like the spiral mode this mode is also aperiodic. The roll mode involves almost a pure roll about the x-axis. The critical state variable is roll rate ( $p$ ).

The final lateral mode is a coupled lateral-directional motion normally referred to as *dutch roll*. This motion is normally oscillatory and involves the state variables  $\beta$ ,  $p$ , and  $r$ . This motion is normally triggered by a sideslip disturbance which causes both yawing and rolling motions. The aircraft continues to roll and yaw similar to the weaving

motions of an ice-skater. The oscillation of this mode may be of high or low frequency and may be lightly or heavily damped. Early aircraft types, with large vertical tails, did not have a dutch roll problem. The motion was more of a flat yaw change with little rolling motion. High performance aircraft with lower directional stability exhibit large amounts of roll and yaw attributable to the dutch roll motion. A lightly damped dutch roll motion will increase the pilots workload during a critical tracking task. Figure 2.4 typifies dutch roll if the aircraft is flying out of the page.

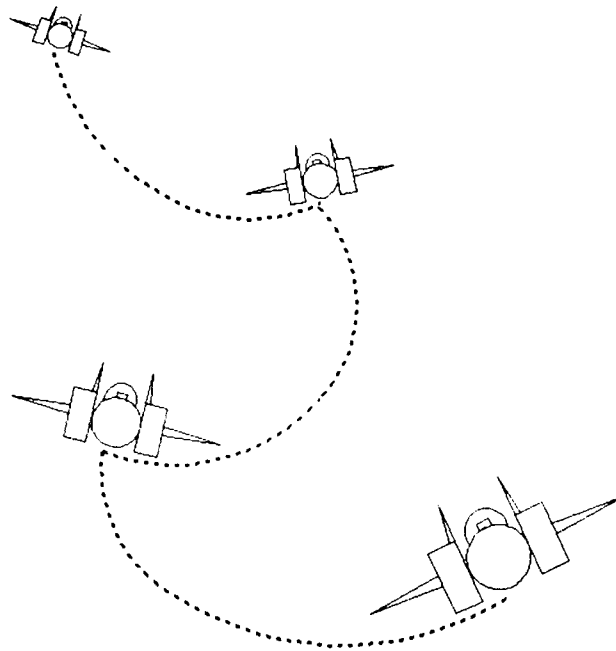


Figure 2.4. Dutch Roll Mode (14:163)

### Bifurcation Analysis

Since wing rock is highly nonlinear we need an efficient analysis strategy to study it's behavior. A number of previous studies have demonstrated that bifurcation analysis

can be used to predict and characterize many nonlinear high angle of attack behaviors of fighter aircraft (3;4;5;21;33). This study uses bifurcation theory to determine aircraft behavior at high AOA. This section contains a brief description of bifurcation theory and demonstrates it's application toward general nonlinear systems. Much of this section was derived from (26;4:6-18). This section will present the concepts of equilibrium, stability and limit cycles. Bifurcation diagrams will be introduced and the three important types of bifurcation branch points will be defined. Periodic solutions to the aircraft equations of motion will also be addressed.

Equilibrium and Stability. Bifurcation theory (which appears in different forms in catastrophe theory, singularity theory and dynamic systems theory) provides an appropriate framework for analyzing nonlinear aircraft equations of motion. In many actual dynamic systems behavior is governed by ordinary differential equations which describe the motion of the various states of the system. Aircraft are prime examples of dynamic systems which may be modeled as a set of differential equations. The aircraft equations of motion can be written in vector form as

$$\dot{u} = f(u,c) \quad (2.1)$$

where the state vector  $u = [\alpha, \beta, v, p, q, r, \theta, \phi]^T$  includes the usual longitudinal and lateral quantities and the parameter vector  $c = [\delta_c, \delta_r, \delta_a]^T$  includes the control surface deflections. This study will mostly be concerned with varying the stabilator angle  $\delta_c$ .

Parameters held fixed include thrust and differential control surface deflections.

A system is said to be at *equilibrium* when it is in a condition of rest or a condition

of uniform motion (steady state flight). Therefore, it follows that equilibrium solutions to the aircraft model equations of motion will satisfy

$$f(u_o, c) = 0 \quad (2.2)$$

The points which satisfy this equation are of particular interest and are called *equilibrium or stationary points*.

The behavior of a system in the neighborhood of an equilibrium point is determined by its *stability*. Stability is defined as the system's tendency to return to the equilibrium point when disturbed. An equilibrium point is *asymptotically* stable if the response to a small disturbance approaches zero as time approaches infinity; it is said to be stable if the response remains small as time approaches infinity; and it is said to be unstable if the response grows without bound as time approaches infinity. Here the term stable includes both asymptotic stability and neutral stability. The local nature of stability is also important to understand. While an equilibrium point may be stable for a disturbance of a certain magnitude within a small neighborhood of the point, it may be unstable for a disturbance of larger magnitude.

To determine the stability of a solution in the vicinity of an equilibrium point the concept of linearized stability is used. For the two-dimensional case our system of equations becomes

$$\begin{aligned} \dot{u}_1 &= f_1(u_1, u_2) \\ \dot{u}_2 &= f_2(u_1, u_2) \end{aligned} \quad (2.3)$$

Taking a Taylor series expansion about an equilibrium point,  $u^o = (u_1^o, u_2^o)$  , and neglecting terms higher than first order,

$$\begin{aligned}\dot{u}_1 &= \frac{\delta f_1}{\delta u_1}(u_1^o, u_2^o)(u_1 - u_1^o) + \frac{\delta f_1}{\delta u_2}(u_1^o, u_2^o)(u_2 - u_2^o) \\ \dot{u}_2 &= \frac{\delta f_2}{\delta u_1}(u_1^o, u_2^o)(u_1 - u_1^o) + \frac{\delta f_2}{\delta u_2}(u_1^o, u_2^o)(u_2 - u_2^o)\end{aligned}\tag{2.4}$$

For a local coordinate system with its origin at  $u^o$  defined by

$$\begin{aligned}h_1 &= u_1 - u_1^o \\ h_2 &= u_2 - u_2^o\end{aligned}\tag{2.5}$$

After substituting the above values of  $h$  our Taylor series expansion becomes

$$\begin{aligned}\dot{h}_1 &= \frac{\delta f_1}{\delta u_1}(u_1^o, u_2^o)h_1 + \frac{\delta f_1}{\delta u_2}(u_1^o, u_2^o)h_2 \\ \dot{h}_2 &= \frac{\delta f_2}{\delta u_1}(u_1^o, u_2^o)h_1 + \frac{\delta f_2}{\delta u_2}(u_1^o, u_2^o)h_2\end{aligned}\tag{2.6}$$

After generalization to an n-dimensional system,

$$\dot{h} = f_u^o h \quad (2.7)$$

here  $f_u^o$  is the Jacobian matrix evaluated at the origin of our local coordinate system  $u^o$ . The problem has now been reduced to a linear system describing the behavior in a small neighborhood close to the equilibrium point. Assuming that  $h$  is of the form  $h = e^{\lambda t} w$ , then the  $n$ -dimensional system takes the form

$$\lambda w = f_u^o w \quad (2.8)$$

which is a general eigenvalue problem where  $\lambda$  is the eigenvalue and  $w$  is the eigenvector. The stability of this linear system and therefore the nonlinear system close to the origin  $u^o$ , is then determined by the sign of the real part of the eigenvalues. If all eigenvalues have zero or negative real parts the equilibrium point is stable. Instability is indicated by any eigenvalue with a positive real part.

The nature of the eigenvalues also determines the type of equilibrium point (ie. node, saddle, focus) and the behavior of solutions near the equilibrium point. Asymptotically stable critical points are called attractors while unstable points are referred to as repellers. The point found in the example is an attractor. A stable limit cycle is another type of attractor.

Limit Cycles. In some physical systems everything does not necessarily tend toward an equilibrium point. There are systems which assume a periodic or cyclic motion. If after some time  $T_0$  a system remains in a cyclic motion with period  $T$ , such that  $u(t) = u(t + T)$  where  $u(t)$  is a solution to equation 2.1, this motion may then be described by a limit cycle. The following figure shows the solution trajectories of a 2-dimensional

system as it leaves an unstable focus and approaches a limit cycle.

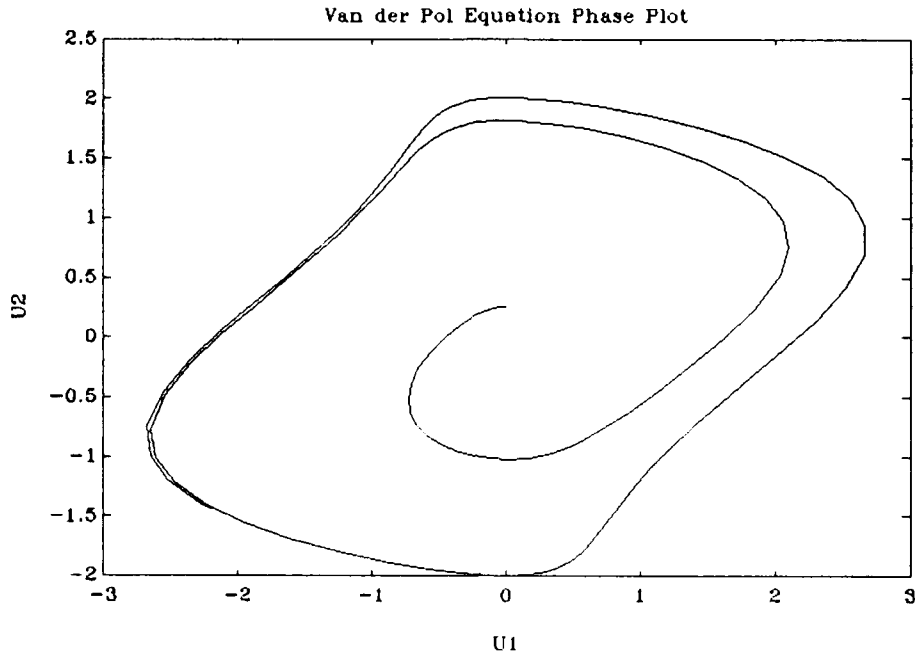


Figure 2.5. Van der Pol Trajectory

This system is a specific case of the Van der Pol equation:

$$\ddot{x} - \sigma(1 - x^2)\dot{x} + x = 0 \quad (2.9)$$

with

$$\sigma = 1$$

$$u_1 = x \quad (2.10)$$

$$u_2 = \dot{u}_1$$

For a stable limit cycle solution trajectories approach from the inside and the outside of the limit. Limit cycles are of particular interest to this study since many nonlinear aircraft motions, including wing rock are represented by limit cycles. The wing rock limit cycle phenomenon begins with some type of asymmetric flow condition. A roll

oscillation amplitude will continue to build if the roll damping is negative. The transient amplitude of the motion will grow gradually over some oscillation cycles because of the roll instability effect at low roll angles. Then at a larger angle there is an increase in effective roll damping which will reduce roll rate and the solution will approach the limit cycle solution (9:921). The following figure illustrates the wing rock limit cycle.

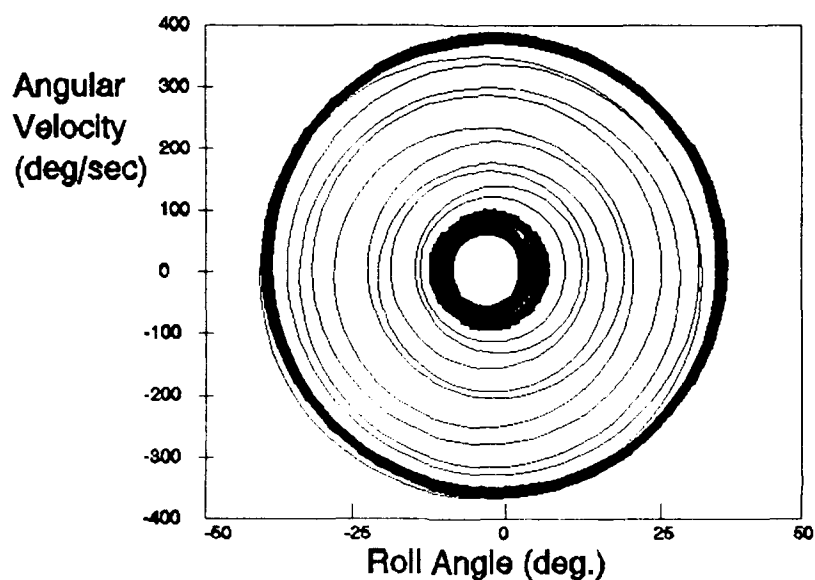


Figure 2.6. Wing Rock Limit Cycle (2:176)

Much like the stability of an equilibrium solution is determined by the eigenvalues of the Jacobian matrix, stability of a periodic solution to the equations of motions are determined by the eigenvalues of the *monodromy matrix*. The monodromy matrix of the periodic solution  $u^*(t)$  with period  $T$  and initial value  $z^*$  defined by the following equation

$$M = \frac{\delta \phi(T; z^*)}{\delta z} \quad (2.11)$$

where  $\phi(t;z)$  is a trajectory which solves equation (2.1) with  $u(0) = \phi$ . One of the eigenvalues of  $M$  is always equal to one. If the moduli of the remaining eigenvalues are all less than or equal to one, the periodic solution is stable. Any eigenvalue with a modulus greater than one indicates instability. The eigenvalues of  $M$  are referred to as *Floquet Multipliers*. The reader is referred to *Waltman* (32) for further information on limit cycles and/or the stability of solutions of differential equations.

Bifurcation Diagrams and Parameters. As presented earlier the aircraft system can be modeled as

$$\dot{u} = f(u,c) \quad (2.12)$$

where  $u$  is the aircraft state vector and  $c$  is the control vector. In this case the control vector contains the control surface deflections as parameters. Other types of control parameters for aircraft would include thrust and weight. The approach followed by bifurcation analysis is to allow one control parameter,  $c_i$ , to vary (in this case  $\delta_c$ ) solving for the equilibrium solutions and/or periodic solutions at each value of  $c_i$ . This type of parameterization permits a greater study of system behavior. These computed solutions (the aircraft states) may then be plotted versus the given control parameter as it is varied. This plot known as a *bifurcation diagram* serves to show all solution branches on a single plot and hence to gain an appreciation for the total solution of the aircraft equations of motion. Typically, in bifurcation diagrams stable portions are shown as solid lines while unstable solutions are depicted with dashed lines. The parameter which is allowed to vary is called the bifurcation parameter. As the bifurcation parameter is varied over a

given range, bifurcation analysis allows us to trace the movement of the equilibrium point. More importantly, for nonlinear systems special points called *branch points* can be located. These points show where the number and stability of solutions to the equations of motion may change or where equilibrium solutions transition to periodic motion. Periodic solutions may also be traced as functions of the bifurcation parameter.

Two types of branch points are important to this study. They are *limit points* and *Hopf Bifurcations*.

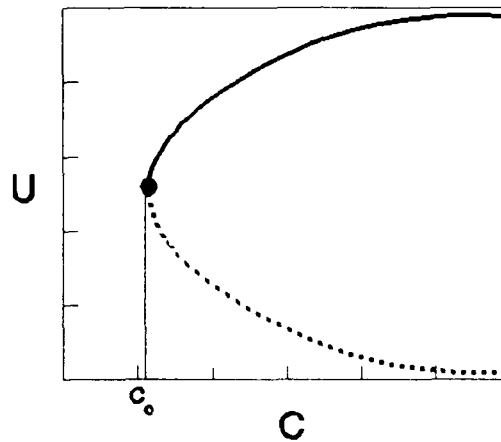


Figure 2.7. Bifurcation Diagram with Limit Point

Limit Points. Limit points occur when one eigenvalue of the Jacobian is zero. The following figure is a bifurcation diagram showing a limit point. Limit points are characterized by having two solutions on one side of  $c_0$  and none on the other side of  $c_0$ , where  $c_0$  is the value of the bifurcation parameter at the limit point.

The branch behaves as:

$$u = tx^2 \quad (2.13)$$

where  $u = c - c_0$  and  $x = u_k(c) - u_k(c_0)$  are local deviation forms of the bifurcation parameter and one of the aircraft state variables and  $t$  is a constant (21:3). Because a limit point occurs as a real eigenvalue moves across the imaginary axis, it usually represents a change in stability and at least one portion of the branch departing the point must be unstable.

Hopf Bifurcations. The branch point previously discussed represents a transition from equilibrium solutions to equilibrium solutions. However, what is of greater significance in nonlinear dynamics is the development of periodic motions (limit cycles). The point at which periodic motions emanate from a branch of stable equilibria is called a Hopf bifurcation. These points occur when a complex conjugate pair of eigenvalues cross the imaginary axis. The Hopf bifurcation behaves as

$$r(u - tr^2) = 0 \quad \text{where} \quad r > 0 \quad (2.14)$$

where  $r$  is the amplitude of oscillation (3:15). The next figure shows a typical Hopf bifurcation.

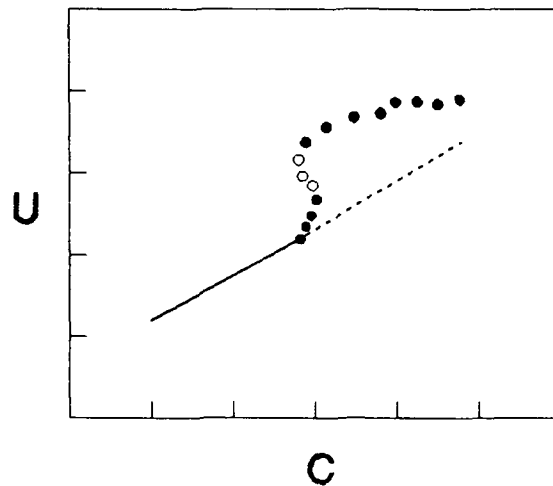


Figure 2.8. Diagram with a Hopf Bifurcation

The Hopf branch is represented by plotting the maximum value the state attains during the limit cycle. Closed circles depict stable portions of the branch while open circles are unstable.

Other bifurcation points can occur but they will not be discussed here as they are not relevant to this study. The interested reader is referred to any of the available texts of bifurcation theory.

#### Bifurcation Software

Obviously, the best way to complete the extensive computations required to perform bifurcation analysis is to employ a numerical routine on a digital computer. There are several software packages available to accomplish the required calculations. This study employed AUTO (6), a FORTRAN package written by E. Doedel. AUTO was selected because it provided the greatest flexibility and required the least modification to fulfill this studies needs.

Program Capabilities. Starting from a known equilibrium point, AUTO first generates the equilibrium branch containing this point. AUTO then computes the points along the equilibrium branch by a process known as *path following*. This process works by repeatedly using known solution points to calculate nearby solutions and thereby trace out the equilibrium branch. Path following is also known as *branch tracing* or *continuation*. As the path following is performed, the software detects and locates limit points, Hopf bifurcations and other bifurcation points. The program then stores information required to allow continuation of new branches that grow from these bifurcation points. AUTO is capable of returning to each of these points and performing a path following along the corresponding solution branches. Resulting equilibrium branch output includes values of all states and parameters.

AUTO also possess the ability to perform path following along periodic branches and thus provide limit cycle data and some measure of the amplitude and period of the oscillatory motion.

This software package also possess the capability of handling a relatively large state space model. AUTO was originally written to support one parameter path following of systems with up to 25 states. The routine was adapted by Beck (4) to accommodate two-parameter continuation of 50 states. The capabilities of AUTO are more than sufficient for this studies requirements.

For the present study, an eigenvalue/eigenvector solver was added to AUTO to determine modal information along the solution branches. The eigenvalue/eigenvector software was taken from *Matrix Eigensystem routines-EISPACK GUIDE* (27) and adapted

to meet this studies needs.

Methods. AUTO requires that the user provide the system state vector,  $u$ , and the system control vector,  $c$ , at a *known* equilibrium point. The user must also supply a subroutine that computes the vector  $f(u,c)$ , the Jacobian matrix  $f_u(u,c)$  and the derivative  $f_c(u,c)$  for a given state vector  $u$  and control parameter vector  $c$ . The user has the option of varying control settings for the analysis.

AUTO employs pseudo arclength continuation (path following) to compute the equilibrium branches.

Differentiating, our system equation becomes

$$df(u,c) = f_u du + f_c dc = 0 \quad (2.15)$$

or

$$du = -f_u^{-1} f_c dc \quad (2.16)$$

An iteration could be used here to solve for the equilibrium branch, however, it would fail at limit points and at bifurcation points because the Matrix  $f_u$  would be singular at these points. To remedy this, a pseudo arclength parameterization is introduced through the equation

$$\theta_u^2 (u - u_o)^T du + \theta_1^2 (c_i - c_{io}) dc - (s - s_o) ds = 0 \quad (2.17)$$

where  $c_i$  is the bifurcation parameter,  $(u_o, c_{io})$  is a previously computed equilibrium point,  $\theta_u$  and  $\theta_c$  are scaling factors and  $s$  is an arclength. This produces a system which is nonsingular at all branch points and can be simply expressed as

$$\left[ \frac{f_u | f_c}{\theta_u^2 (u - u_o)^T | \theta_c^2 (c_i - c_{io})} \right] \left[ \frac{du}{dc} \right] = \left[ \frac{\theta}{(s - s_o) ds} \right] \quad (2.18)$$

therefore, given the starting equilibrium point, AUTO determines a null vector of the matrix  $[ f_u | f_c ]$  to find a tangent to the equilibrium branch. This tangent is used to make an initial approximation to the second solution point. A Newton iteration form of the above equation is used to locate the next equilibrium point accurately. Further branch points are determined by extrapolating two previous points linearly and using Newton iterations to locate the point accurately.

As the path following is carried out, the eigenvalues and eigenvectors are computed. Real or complex eigenvalues crossing the imaginary axis (corresponding to an equilibrium bifurcation point or a Hopf bifurcation point) are detected by checking the real parts of every eigenvalue. The determinant of the matrix in the above equation is also calculated as the bifurcation parameter is varied. Sign changes of this determinant indicate a simple bifurcation point. AUTO then locates crossing points accurately and stores the appropriate data to permit restart of additional solution branches.

AUTO uses a similar method for path following of periodic branches from limit points and Hopf bifurcations. However, the program sets up the periodic branch

continuation as a two-point boundary value problem. For further development of these methods the reader is referred to Doedel (6).

### Aircraft Description

McDonnell Douglas F-15 Eagle. This study uses three aircraft to validate its findings. The first is the F-15 *Eagle* (30). The Eagle is a two engine supersonic aircraft built by the McDonnell Aircraft Company primarily as an air-superiority fighter. The aircraft is characterized by a high-mounted swept wing and twin vertical stabilizers. In addition to the air superiority version, a dual-role (air-to-air and deep strike) variant has been introduced along with an experimental short takeoff and landing model. This study models the aircraft in a clean configuration with no external stores with gear, flaps and speed brake retracted. Also thrust will be held constant at 8300 pounds and the aircraft's mass and inertia properties are assumed constant. Dimensional, inertia and weight data for the F-15 are included in Appendix A.

For maneuvering, the F-15 has three independent sets of control surfaces. It has left and right horizontal stabilators, left and right ailerons and left and right rudders. Stabilator movement consists of both symmetrical and differential (split) deflections. Symmetric stabilator deflection,  $\delta_e$ , is the primary method of pitch control. Roll control is derived through the ailerons,  $\delta_a$ , and yaw control is provided through rudder deflection,  $\delta_r$ . The split stabilator deflection, referred to as differential tail,  $\delta_{dt}$ , is used to assist in roll control and, disregarding control augmentation system inputs, is directly

proportional to aileron deflection (14:15). Differential deflections allow for increased maneuverability during combat and provide increased flexibility for optimal control system augmentation.

In this study, control surface deflection limits are neglected. The aircraft model used permits full control surface deflection so that continuation of equilibrium and periodic bifurcation branches can occur. If these limits were included it would prevent location of many valid equilibrium and periodic solutions which are found when a branch passes outside the limits of permissible control deflections and then returns to within the limits. Although limiters are neglected in the model they should be considered when analyzing the results therefore control surface deflection limits and sign conventions are identified in Appendix A. The flight envelope considered by this test is well within the capabilities for the F-15. The elimination of control limits from the model will have no bearing on the conclusions drawn by this study. The controls for the F-15 consist of a primary mechanical control system operating in parallel with an electronic dual-channel three-axis control augmentation system (CAS) (14:20). The pilot commands pitch, roll and yaw through longitudinal control stick and rudder pedal deflections, respectively. These controls are connected through a series of actuators. The CAS uses angular velocity feedback to improve stability. This system also includes a stall inhibitor system to prevent onset of stall and an aileron-rudder interconnect to allow for easier turn coordination and improved lateral-directional flying qualities.

McDonnell Douglas F-4 Phantom. The second aircraft involved in this study is the McDonnell Douglas F-4 Phantom II. The *Phantom* is a two-seat, tandem, supersonic,

long range, all-weather, fighter-bomber currently being phased out of service with the U.S. Air Force. The Phantom has been employed in every fighter role including air superiority, air interdiction, strike and suppression of enemy air defenses. Over 1000 of this type are still in service with U. S. allies.

The aircraft thrust is provided by two axial-flow turbojet engines with variable stators and variable afterburner. Two independent hydraulic control systems provide power to control the F-4. Longitudinal control is provided by an all movable horizontal tail. Lateral control is provided by a combination of spoilers and ailerons. The ailerons deflect downward only; the spoilers deflect upward only. The left aileron and right spoiler operate simultaneously, as do the right aileron and left spoiler. Directional control is provided by a conventional rudder. A simple spring/damper control system provides feel to the pilot. The F-4 uses a three axis stability augmentation system to increase aircraft stability. The three channels of stability are all independently cockpit selectable and F-4 pilots often disengage the roll stability augmentation system to increase roll performance. The physical characteristics and the control deflection limits of the F-4 are shown in appendix B.

Northrop T-38 Talon. The third aircraft involved in this study is the Northrop T-38 Talon (31). The *Talon* is a two-seat, supersonic jet trainer currently in service with the U.S. Air Force. The T-38 is powered by two General Electric J85-G-5 turbojet engines rated at 2,050 LBS thrust (military) and 2,900 LBS thrust in afterburner.

The Talon has a fully powered irreversible control system with all-movable horizontal tail. All control surfaces are operated by two independent hydraulic systems.

Artificial feel is provided in the longitudinal and lateral axis with a yaw damper to control yaw oscillations. The horizontal tail system's artificial feel system consists of a bungee and a bobweight. Artificial feel for the ailerons and rudder is achieved by means of bungees. Maximum rudder deflection is reduced with the landing gear retracted to prevent structural damage to the vertical tail. Trim is provided by electric actuators that reposition the neutral position of the bungees. The flaps are mechanically interconnected to the horizontal tail to automatically change its angle to the trim position when the flaps are actuated.

The T-38, F-4 and F-15 were examined for several reasons. First, the actual aircraft are designed to fly safely at moderately high angles of attack however, all three aircraft exhibit wing rock above approximately 10 degrees AOA. Second, these aircraft are statically stable at lower angles-of-attack. Therefore, it is possible to study basic stable motions of these aircraft without an added stabilizing control system. Third, extensive and well validated F-15 and F-4 aerodynamic databases were available. Finally, as part of the AFIT/TPS joint program a fully instrumented T-38A and RF-4C were available to validate portions of this study by flight test. A full description of these aircraft maybe found in their respective flight manuals. Appendix C contains basic characteristics of the T-38.

### Basic Aircraft Model

Aircraft Equations of Motion. The equations of motion used in this study are nonlinear. These nonlinear relationships are based on the following assumptions:

1. The aircraft is a rigid body.
2. The aircraft has constant mass and mass properties.
3. The x-z plane is a plane of symmetry.
4. The Earth provides a fixed reference frame in space.

Based on the above assumptions, the six-degree-of freedom equations of motion become  
(16:233)

$$X = m[\dot{u} + qw - rv + g \sin \theta] \quad (2.19)$$

$$Y = m[\dot{v} + ru - pw - g \cos \theta \sin \phi] \quad (2.20)$$

$$Z = m[\dot{w} + pv - qu - g \cos \theta \cos \phi] \quad (2.21)$$

$$L = \dot{p}I_x - \dot{r}I_{xz} + qr(I_z - I_y) - pqI_{xz} \quad (2.22)$$

$$M = \dot{q}I_y + pr(I_x - I_z) - r^2I_{xz} + p^2I_{xz} \quad (2.23)$$

$$N = \dot{r}I_z - \dot{p}I_{xz} + pq(I_y - I_x) + qrI_{xz} \quad (2.24)$$

where

$m$  = aircraft mass

$X, Y, Z$  = aerodynamic forces

$L, M, N$  = aerodynamic moments

$u, v, w$  = velocity components

$p, q, r$  = angular velocities

$I_{xx}, I_{yy}, I_{zz}$  = moments of inertia about the body axes

$I_{xz}$  = cross-product of inertia for the x-z plane

$\theta$  = pitch angle

$\phi$  = bank angle

$g$  = gravitational force

The aircraft data base used in this study presents data in the aircraft body axis system.

The aircraft body axes and orientations are defined in figure 2.9 and the gravity vector is related to the body axes as shown in figure 2.10.

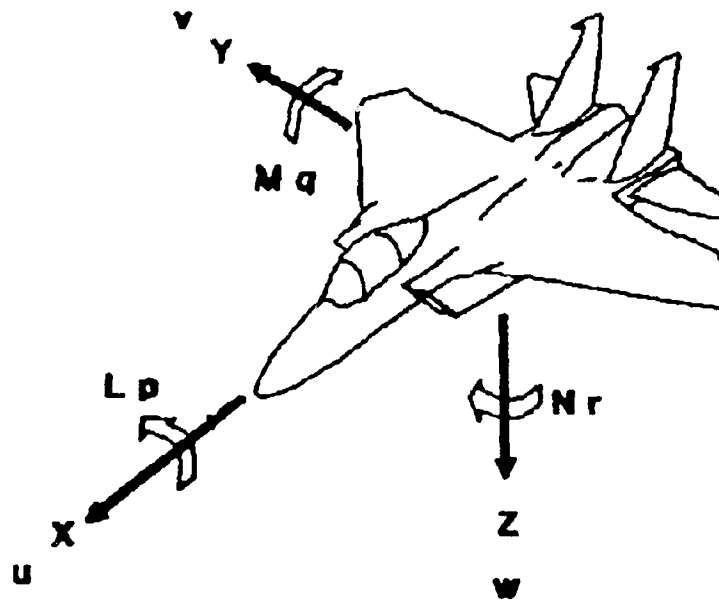


Figure 2.9. Aircraft Body Axes (4:28)

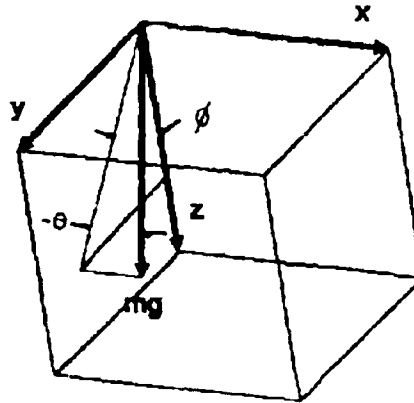


Figure 2.10. Gravity Vector and Body Axes (16:222)

In addition, to the equations of motion the following kinematic relations are necessary (16:223):

$$\dot{\phi} = p + q \tan \theta \sin \phi + r \tan \theta \cos \phi \quad (2.25)$$

$$\dot{\theta} = q \cos \phi - r \sin \phi \quad (2.26)$$

Heading angle need not be considered since it is not dependent upon aerodynamics and is decoupled from the other equations.

The true velocity,  $V_u$ , angle of attack,  $\alpha$ , and sideslip angle,  $\beta$ , are defined as shown

in figure 2.11.

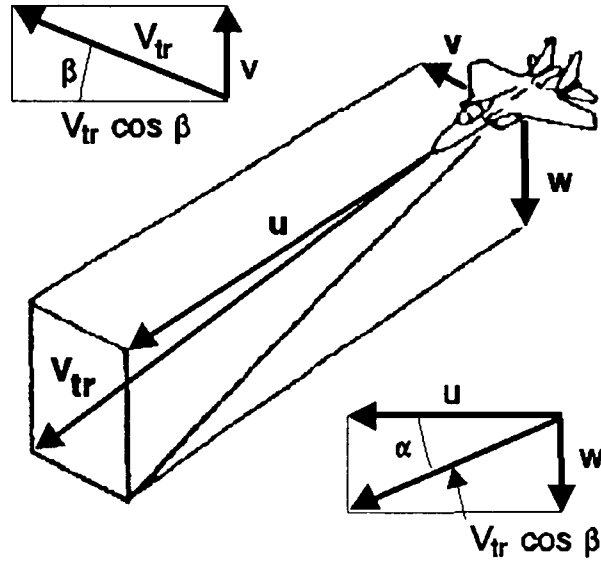


Figure 2.11. Aircraft Velocity Components (4:30)

Therefore the following relationships hold:

$$v = V_{tr} \sin \beta \quad (2.28)$$

$$w = V_{tr} \sin \alpha \cos \beta \quad (2.29)$$

$$\dot{u} = \dot{V}_{tr} \cos \alpha \cos \beta + V_{tr} (-\dot{\alpha} \sin \alpha \cos \beta - \dot{\beta} \cos \alpha \sin \beta) \quad (2.30)$$

$$\dot{v} = \dot{V}_{tr} \sin \beta + V_{tr} \dot{\beta} \cos \beta \quad (2.31)$$

$$\dot{w} = \dot{V}_{tr} \sin \alpha \cos \beta + V_{tr} (\dot{\alpha} \cos \alpha \cos \beta - \dot{\beta} \sin \alpha \sin \beta) \quad (2.32)$$

$$\dot{w} = \dot{V}_r \sin \alpha \cos \beta + V_r (\dot{\alpha} \cos \alpha \cos \beta - \dot{\beta} \sin \alpha \sin \beta) \quad (2.32)$$

In addition, the aerodynamic force and moment coefficients can be represented as follows:

$$C_x = \frac{X}{QS} \quad (2.33)$$

$$C_y = \frac{Y}{QS} \quad (2.34)$$

$$C_z = \frac{Z}{QS} \quad (2.35)$$

$$C_l = \frac{L}{QSb} \quad (2.36)$$

$$C_m = \frac{M}{QSc} \quad (2.37)$$

$$C_n = \frac{N}{QSb} \quad (2.38)$$

where  $Q$  is the dynamic pressure,  $S$  is the wing planform area,  $b$  is the wing span and  $c$  is the mean aerodynamic chord. Substituting equations 2.27-2.35 into equations 2.19-2.21 and solving simultaneously  $d\alpha/dt$ ,  $d\beta/dt$ ,  $dV_r/dt$  yields the following equations.

$$\dot{\alpha} = \dot{q} - \left[ \frac{QS}{mV_r} C_x - \frac{g}{V_r} \sin\theta + r \sin\beta \right] \sin\alpha \sec\beta \quad (2.39)$$

$$+ \left[ \frac{QS}{mV_r} C_z + \frac{g}{V_r} \cos\theta \cos\phi - p \sin\beta \right] \cos\alpha \sec\beta$$

$$\dot{\beta} = - \left[ \left[ \frac{QS}{mV_r} C_x - \frac{g}{V_r} \sin\theta \right] \sin\beta + r \right] \cos\alpha$$

$$+ \left[ \frac{QS}{mV_r} C_y + \frac{g}{V_r} \cos\theta \sin\phi \right] \cos\beta \quad (2.40)$$

$$- \left[ \left[ \frac{QS}{mV_r} C_z + \frac{g}{V_r} \cos\theta \cos\phi \right] \sin\beta - p \right] \sin\alpha$$

$$\dot{V}_r = V_r \left[ \frac{QS}{mV_r} C_x - \frac{g}{V_r} \sin\theta \right] \cos\alpha \cos\beta$$

$$+ V_r \left[ \frac{QS}{mV_r} C_y + \frac{g}{V_r} \cos\theta \sin\phi \right] \sin\beta \quad (2.41)$$

$$+ V_r \left[ \frac{QS}{mV_r} C_z + \frac{g}{V_r} \cos\theta \cos\phi \right] \sin\alpha \cos\beta$$

Using equations 2.36-2.38, equations 2.22 and 2.24 can be solved simultaneously for  $dp/dt$  and  $dr/dt$  and 2.23 can be solved directly for  $dq/dt$  to give

$$\dot{p} = \left[ - \left[ \frac{I_z - I_y}{I_x} + \frac{I_{xz}^2}{I_x I_z} \right] q r + \left[ 1 - \frac{I_y - I_x}{I_z} \right] \frac{I_{xz}}{I_x} p q \right] + \left[ \frac{Q S b}{I_x} \left[ C_l + \frac{I_{xz}}{I_z} C_n \right] \right] \left[ 1 - \frac{I_{xz}^2}{I_x I_z} \right]^{-1} \quad (2.42)$$

$$\dot{q} = \frac{Q S c}{I_y} C_m + \frac{I_z - I_x}{I_y} p r + \frac{I_{xz}}{I_y} (r^2 - p^2) \quad (2.43)$$

$$\dot{r} = \left[ \frac{I_{xz}^2}{I_x I_z} - \frac{I_y - I_x}{I_z} \right] p q - \left[ 1 + \frac{I_z - I_y}{I_x} \right] \frac{I_{xz}}{I_z} q r + \frac{Q S b}{I_z} \left[ \frac{I_{xz}}{I_x} C_l + C_n \right] \left[ 1 - \frac{I_{xz}^2}{I_x I_z} \right]^{-1} \quad (2.44)$$

The system now consists of equations 2.39-2.44 combined with the pitch rate and roll rate expressions (2.25-2.26).

The first order system follows

$$\dot{u} = f(u, c) \quad (2.45)$$

where  $u$  and  $c$  are the vectors:

$$\begin{aligned} u &= [\alpha, \beta, p, q, r, \theta, \phi, V_{tr}]^T \\ c &= [\delta_e, \delta_r, \delta_a]^T \end{aligned} \tag{2.46}$$

The dependence on  $c$  comes into effect through the force and moment coefficients which are functions of  $u$  and  $c$ . This set of equations is identical to the set used by Planeaux (21) and Beck (4). To completely define the eight-state model we must develop the force and moment coefficients.

Aerodynamic Force and Moment Coefficients. The expansions of the aerodynamic force and moment coefficients were extracted from a McDonnell Aircraft Company F-15 simulator program. The coefficients were obtained from simulator data (combined wind tunnel and flight test data) tabulated for Mach numbers from .3 to 2.5 and from 0 to 80,000 feet. Mach number and altitude dependence had been eliminated by selecting data at .6 Mach and 20,000 ft. The data has been curve fit to multivariable polynomials to provide a more efficient model. The equations are as follows:

$$C_x = C_L(\alpha, \delta_e) \sin \alpha - C_D(\alpha, \delta_e) \cos \alpha + \frac{T}{(QS)} \tag{2.47}$$

$$C_y = C_{y_\beta}(\alpha, |\beta|, \delta e) + C_{y_{\delta a}}(\alpha) \delta a + C_{y_{\delta r}}(\alpha, |\delta r|) \delta r \\ + \left[ \frac{b}{2V_{tr}} \right] [C_{y_r}(\alpha)r + C_{y_p}(\alpha)p] \quad (2.48)$$

$$C_z = -C_L(\alpha, \delta e) \cos \alpha - C_D(\alpha, \delta e) \sin \alpha \quad (2.49)$$

$$C_l = c_{l_\beta}(\alpha, |\beta|) + C_{l_{\delta a}}(\alpha, \delta e) \delta a + C_{l_{\delta r}}(\alpha, |\delta r|) \delta r \\ + \left[ \frac{b}{2V_{tr}} \right] [C_{l_p}(\alpha)p + C_{l_r}(\alpha)r] \quad (2.50)$$

$$C_m = C_{m_\theta}(\alpha, \delta e) + \left[ \frac{c}{2V_{tr}} \right] C_{m_q}(\alpha)q + \frac{T\delta t}{QSc} \quad (2.51)$$

$$C_n = C_{n_\beta}(\alpha, |\beta|, \delta e) + C_{n_{\delta a}}(\alpha) \delta a + C_{n_{\delta r}}(\alpha, |\beta|, |\delta r|, \delta e) \delta r \\ + \left[ \frac{b}{2V_{tr}} \right] [C_{n_p}(\alpha)p + C_{n_r}(\alpha)r] \quad (2.52)$$

Each of the aerodynamic coefficients and stability derivatives in the above equations are functions of the aircraft states and the control surface deflections shown. For a more detailed description of the aerodynamic coefficient development, see (3, 10-19). With these coefficients, the eight-state F-15 model is fully developed.

### Starting Point Selection

A single solution to the system  $f(u,c) = 0$  is required to begin the bifurcation continuation process. Straight, wings-level flight was chosen as a starting point because equilibrium solutions to the equations of motion can be easily found. Based on these assumptions most of the states are zero. By then simplifying the system and specifying one of the remaining states, the system can be solved simultaneously. The specified parameter chosen was angle-of-attack and its initial value was  $10^\circ$ .

### III. Analytical Results

#### Bifurcation Analysis

The bifurcation parameter chosen for this study was stabilator deflection. Angle-of-attack was increased in small steps as stabilator deflection was increased (in the negative direction) from the starting point. This results in a straight pull-up maneuver being *flown* by the model. A one parameter change of stabilator angle was chosen to hopefully isolate the motion producing wing rock at a condition that would decouple the longitudinal and lateral terms, this simplifies the task of determining the critical components involved in triggering the oscillating motion. The point at which wing rock begins will be referred to as the *trigger point*.

The bifurcation diagram of angle-of-attack for the stabilator sweep is shown in figure 3.1. Branch 1, the branch continued from the initial starting point, has zero lateral states ( $\beta, p, q, r$ ) along its entire length. Branches 2 through 5, which all result from a pitchfork bifurcations, have nonzero lateral states and each represents two branches which are symmetric with respect to the X-Z plane. This can be seen in the  $\beta$  diagram, figure 3.2.

The periodic branch emanating from the Hopf bifurcation on branch 1 is also shown on figure 3.1.

If we assume that the aircraft is in equilibrium at the starting point of  $\alpha$  equal to

10 degrees then as the stabilator deflection is increased (more negative) statically the equilibrium point progresses along branch 1. This would be true assuming no disturbance such as a wind gust is large enough to result in a jump to another stable state along another equilibrium branch or periodic branch. As the stabilator deflection reaches the value at which the Hopf bifurcation occurs, branch 1 becomes unstable.

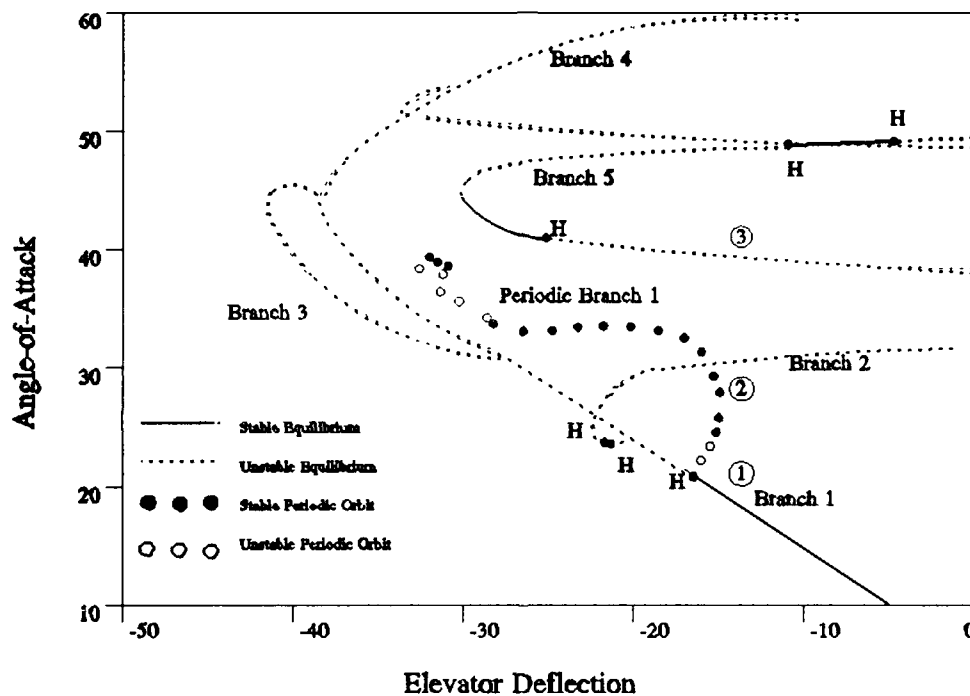


Figure 3.1. Alpha Bifurcation Diagram for F-15

As explained in Chapter 2, a Hopf bifurcation occurs when a complex conjugate pair of poles crosses the imaginary axis into the right half plane. The unstable equilibrium is an unrealizable state since the smallest disturbance will cause the state trajectory to

diverge from equilibrium. Therefore, as the stabilator deflection increases past the critical value at the Hopf bifurcation point, a jump must occur to another attractor, in this case, to the limit cycle represented by periodic branch 1 at this elevator deflection. The phenomenon which causes this jump occurs during the transition from the stable equilibrium portion of branch 1 to the stable limit cycle portion of periodic branch 1.

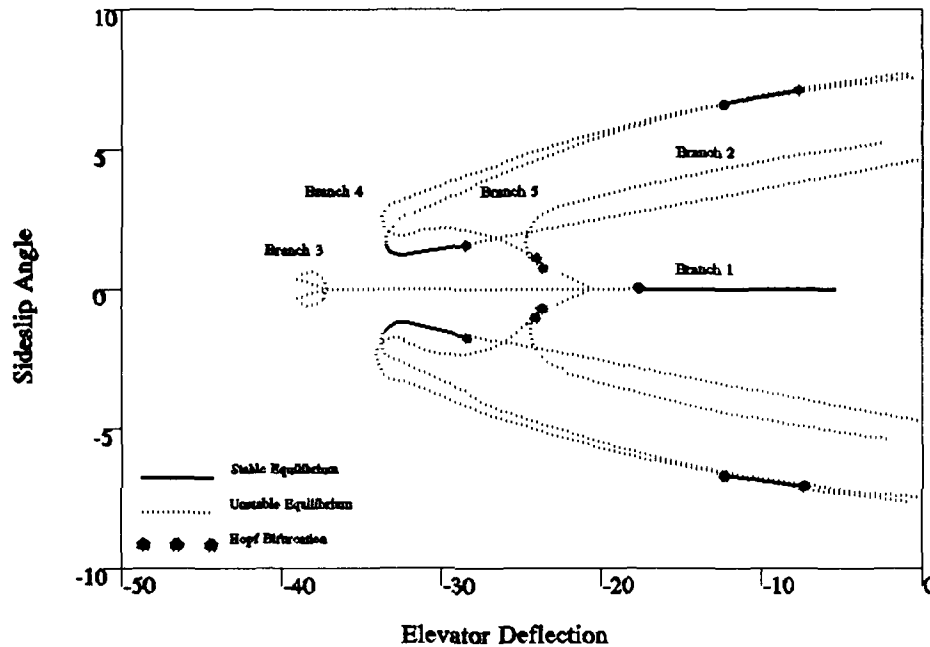


Figure 3.2. Beta Bifurcation Diagram for F-15

This jump actually represents the onset of wing rock and the trigger point is the Hopf bifurcation point located on branch 1. This point occurs at  $\alpha$  equals 21 degrees. Wing rock begins here, and we will demonstrate later on that this coincides with the complex conjugate pair of dutch roll eigenvalues migrating into the right half plane. This point will be critical to the remainder of the analysis. The state values at this Hopf

bifurcation point are presented in table 3.1. These findings agree reasonably well with previous F-15 flight test results (1:50) for Mach equal to .6. These test results are shown in figure 3.3.

Table 3.1. State Values at Hopf Point for F-15

Alpha	Beta	Roll Rate	Pitch Rate	Yaw Rate	Theta	Phi	V True
21°	0	0	0	0	13°	0	277 ft/sec

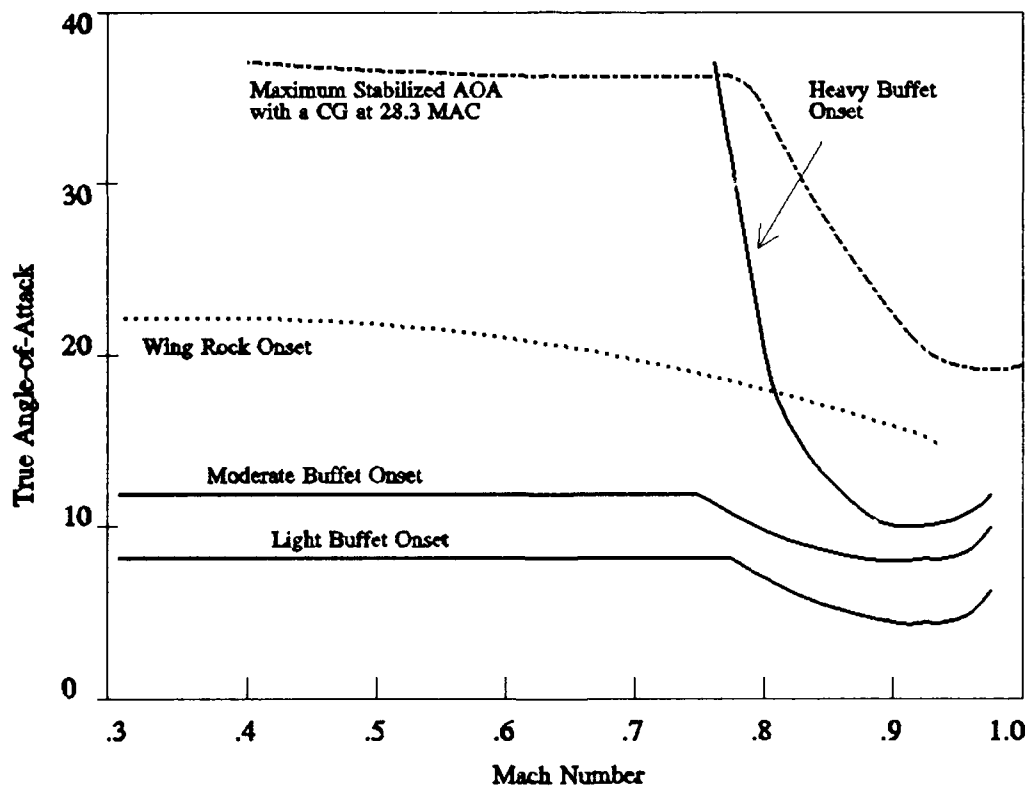


Figure 3.3. F-15 Flight Test Results (1:50)

### Eigenvalue Analysis

The AUTO routine was modified such that the eigenvalues and eigenvectors of the state matrix at all solution points were returned in addition to the bifurcation data.

Figure 3.4 shows the eigenvalues at the starting point, alpha equal 10 degrees.

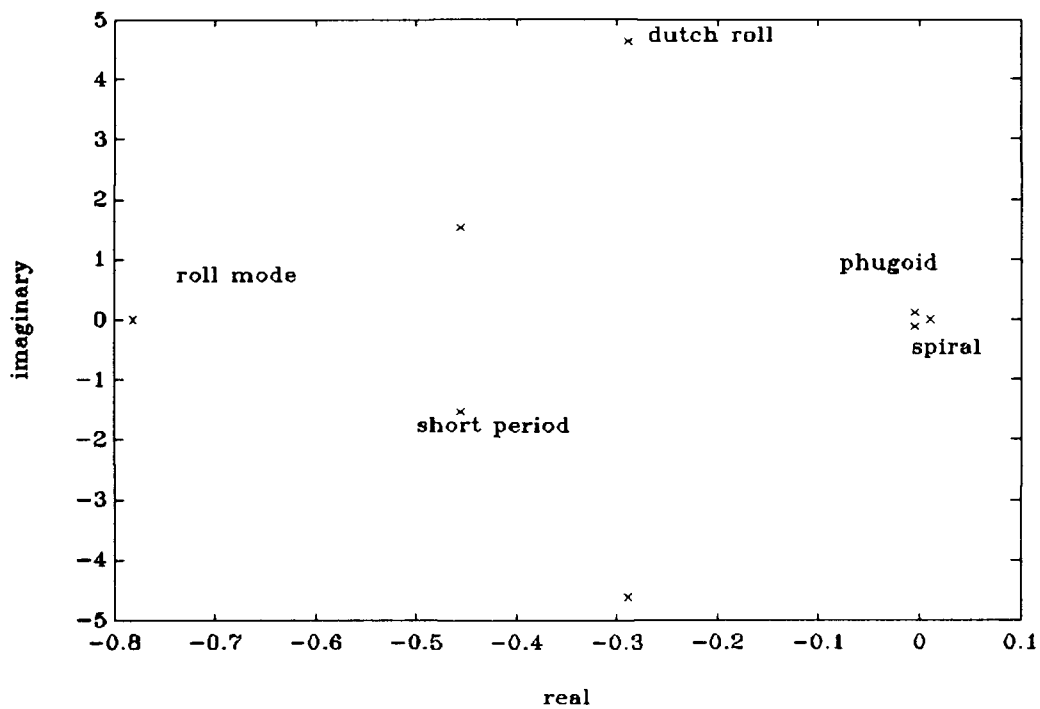


Figure 3.4. Eigenvalues at Alpha = 10° for F-15

The F-15 displays the classic longitudinal and lateral stability modes of a conventional aircraft design. At this point the short period and phugoid motions (longitudinal modes)

exhibit the following characteristics:

Table 3.2. Longitudinal Mode Characteristics for F-15

	Frequency (/sec)	Damping	Time to 1/2 amplitude (sec)
Short Period	1.6	.28	1.55
Phugoid	.11	.048	131

The values in table 3.2 reflect typical longitudinal aircraft behavior. The short period exhibits a higher frequency and greater damping when compared to the phugoid. This is characteristic of an aircraft that will respond well to a stabilator input with minimal overshoot. The phugoid is characterized by a low frequency and is very lightly damped. This does not normally present a problem because phugoid motion occurs so slowly that the pilot can easily negate the disturbance with small control movements.

The lateral modes behave as follows:

Table 3.3 Lateral Mode Characteristics for F-15

	Frequency (/sec)	Damping	Time to 1/2 Amplitude (sec)	Time Constant (sec)
Dutch Roll	4.63	.06	2.4	
Spiral Mode			178.5*	250
Roll Mode			1.28	.883

\*Spiral mode is unstable. This value represents time to double.

Note that for the F-15 at 10 degrees angle-of-attack the spiral mode is unstable. This is not uncommon for a conventional design. Table 3.4 shows the eigenvalues for  $\alpha = 10$ , 21, and 30 degrees.

Table 3.4. Eigenvalues at  $\alpha$  equal 10, 21 and 30 Degrees for F-15

	Aplha = 10°	Alpha = 21°	Alpha = 30°
Short Period Mode	$-.46 \pm 1.5i$	$-.38 \pm 1.3i$	$-.23 \pm 1.17i$
Phugoid Mode	$-.005 \pm .11i$	$-.037 \pm .15i$	$-.077 \pm .16i$
Dutch Roll Mode	$-.29 \pm 4.6i$	$0.0 \pm 2.26i$	$.456 \pm .96i$
Roll Mode	$-.763$	$-.189$	$-.152$
Spiral Mode	$.0024$	$-.544$	$-1.11$

The 21 degree case shows the point where wing rock is triggered. As can be seen in table 3.4 the dutch roll eigenvalues are on the imaginary axis at this point and migrate into the right half plane as alpha increases. This is easier to see in figure 3.5 which depicts a conventional root locus plot for alpha varying from 10 to 30 degrees. Throughout this angle-of-attack change, the plot shows that as alpha is increased the short period mode initially becomes more stable then it moves toward the right half plane but at alpha equal 30 degrees the short period characteristics ( $\omega_{sp}=1.19, \zeta_{sp}=.2$ ) are still respectable. The phugoid mode moves toward increased stability during the alpha

increase. From figure 3.5 it is concluded that the longitudinal modes have little if any effect on the wing rock behavior.

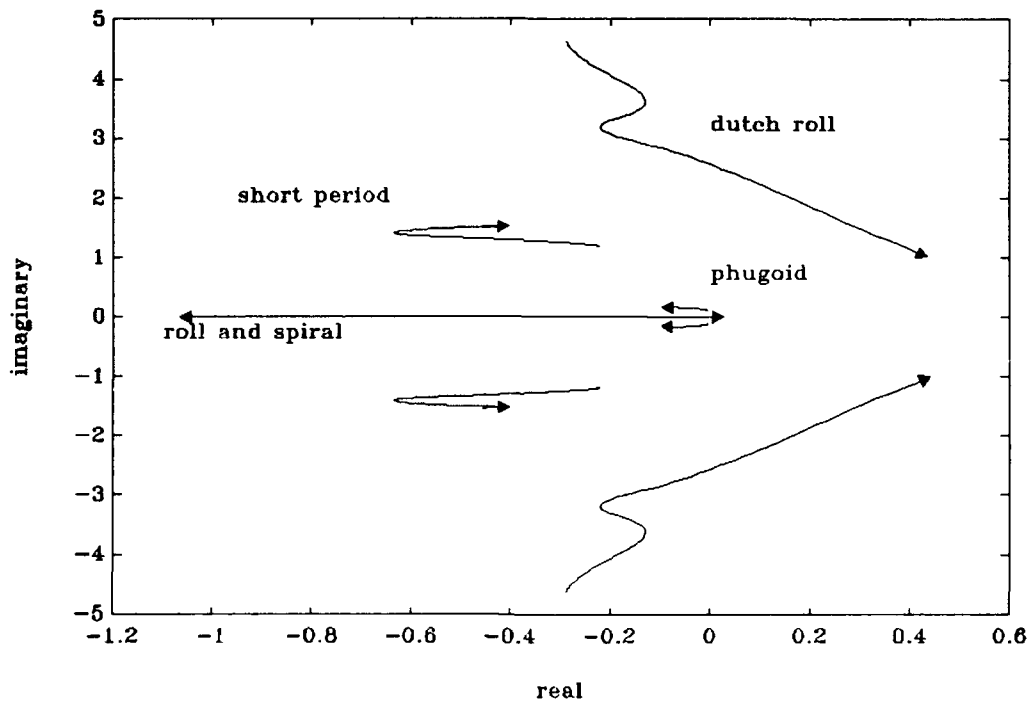


Figure 3.5. Root Locus For F-15 Varying Alpha

Figure 3.6 shows the lateral dutch roll and roll modes while figure 3.7 shows the dutch roll mode and the spiral mode. The data is presented in this method to avoid confusion between the roll mode and spiral mode as they migrate along the real axis.

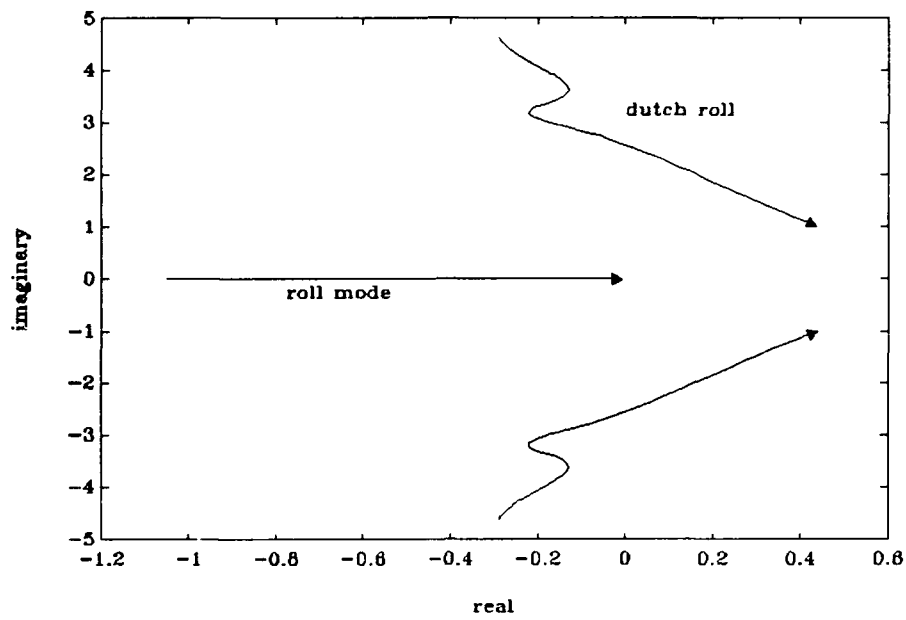


Figure 3.6. Dutch Roll and Roll Modes for F-15

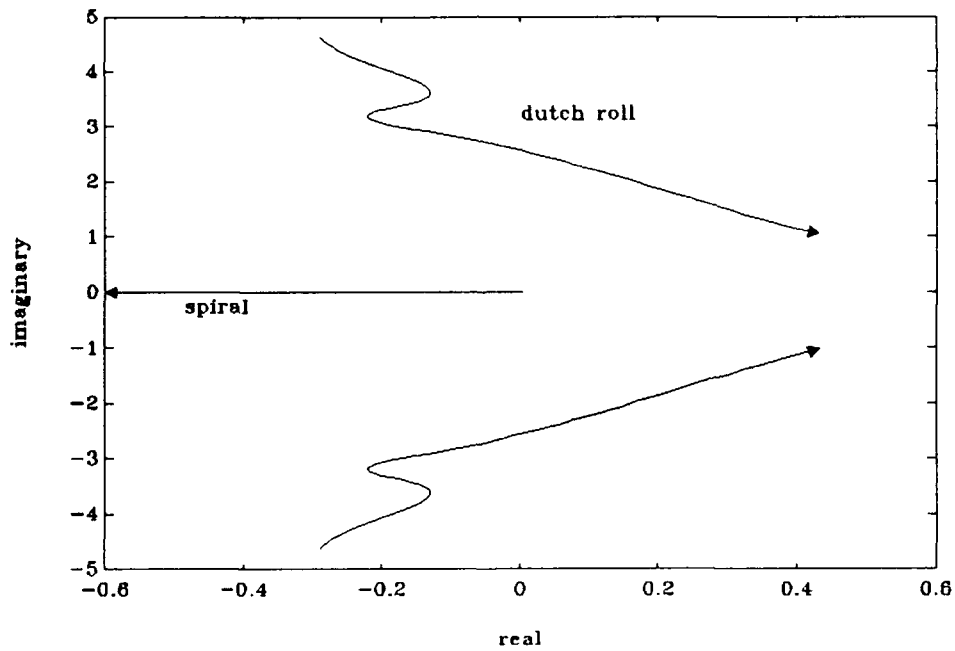


Figure 3.7. Dutch Roll and Spiral Modes For F-15

As can be seen the roll mode moves toward the origin and the spiral mode moves into the left half plane and continues toward increasing stability. The roll mode does not cross into the right half plane over the angle-of-attack range. The dutch roll mode on the other hand, moves toward the right half plane as  $\alpha$  is increased. The motion is neutrally stable at  $\alpha$  equal 21 degrees and becomes unstable shortly thereafter. The point of neutral stability coincides with the Hopf bifurcation point on branch 1 (figure 3.1). The dutch roll mode continues further into the left half plane as  $\alpha$  is increased. From the lateral root loci it appears that wing rock is an unstable dutch roll motion. At low angles-of-attack, dutch roll is normally approximated by a flat motion which does not contain much roll angle change. As  $\alpha$  is increased previous research has shown that this motion becomes predominantly a roll oscillation with little yaw change (19:14). Thus we would expect that the eigenvector data would show that the critical states involved in this unstable motion are  $\beta$ ,  $p$ ,  $\phi$ .

#### Linearization Around the Trigger Point

In order to derive an expression that would indicate that wing rock has been triggered the nonlinear equations of motion have been linearized about the solution point which places the dutch roll eigenvalues on the imaginary axis (Hopf bifurcation point). The linearization process was discussed in Chapter 2 and won't be expanded upon here. Following are the linearized equations:

$$\Delta \dot{\alpha} = \left[ \frac{g}{V_o} (\sin \theta_o \cos \alpha_o - \cos \theta_o \sin \alpha_o) + \frac{QS}{mV_o} (C_{z_s} \cos \alpha_o - C_{x_s} \sin \alpha_o) \right] \Delta \alpha$$

$$+ \Delta q + \left( \frac{g}{V_o} \cos \theta_o \sin \alpha_o - \frac{g}{V_o} \sin \theta_o \cos \alpha_o \right) \Delta \theta$$
(3.1)

$$\Delta \dot{\beta} = \left[ \frac{g}{V_o} (\sin \theta_o \cos \alpha_o + \sin \alpha_o \cos \theta_o) + \frac{QS}{mV_o} C_{y_\beta} \right] \Delta \beta$$

$$+ \left[ \frac{QS}{mV_o} C_{y_p} + \sin \alpha_o \right] \Delta p + \cos \alpha_o \Delta r + \frac{g}{V_o} \cos \theta_o \Delta \phi$$
(3.2)

$$\Delta \dot{p} = A((C_{L_a} + BC_{N_a}) \Delta \alpha + (C_{L_b} + BC_{N_b}) \Delta \beta + (C_{L_p} + BC_{N_p}) \Delta p$$

$$+ (C_{L_r} + BC_{N_r}) \Delta r + (C_{L_v} + BC_{N_v}) \Delta V)$$
(3.3)

$$\Delta \dot{q} = \frac{QSc}{I_z} (C_{M_a} \Delta \alpha + C_{M_q} \Delta q + C_{M_v} \Delta V)$$
(3.4)

$$\Delta \dot{r} = A((BC_{I_b} + C_{N_b}) \Delta \beta + (BC_{I_p} + C_{N_p}) \Delta p$$

$$+ (BC_{I_r} + C_{N_r}) \Delta r + (BC_{I_v} + C_{N_v}) \Delta V)$$
(3.5)

For the angular rate equations (3.3-3.5) A and B are defined in equation 3.6 and will remain as such throughout the remainder of this document.

$$A = \frac{\frac{QSb}{I_x}}{\left[1 - \frac{I_{xz}^2}{I_x I_z}\right]} \quad (3.6)$$

$$B = \frac{I_{xz}}{I_x}$$

$$\Delta \dot{\theta} = \Delta q \quad (3.7)$$

$$\Delta \dot{\phi} = \Delta p \quad (3.8)$$

$$\begin{aligned} \Delta \dot{V} = & \left[ (g \sin \theta_o \sin \alpha_o + g \cos \theta_o \cos \alpha_o) + \frac{QS}{m V_o} (C_{x_a} \cos \alpha_o + C_{z_a} \sin \alpha_o) \right] \Delta \alpha \\ & + (-g \cos \theta_o \cos \alpha_o - g \sin \alpha_o \sin \theta_o) \Delta \theta \end{aligned} \quad (3.9)$$

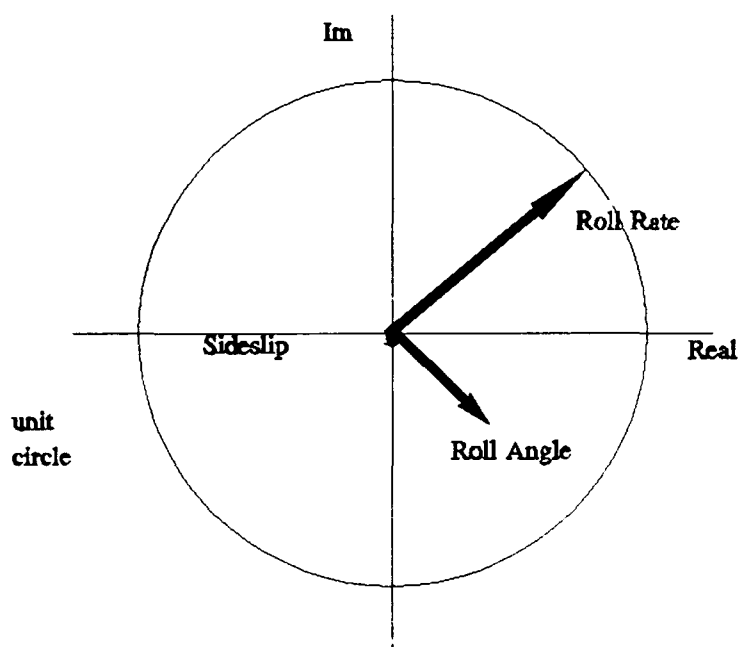
The three steady state conditions of  $\alpha_o$ ,  $\theta_o$ , and  $V_o$  have been left as variables at this point to allow their influence to be seen in expression development.

#### Eigenvector Analysis

For this study the AUTO routine was modified to produce eigenvector data at each solution point. Figure 3.8 shows the relationship of the relative magnitudes of each of

the components of the dutch roll eigenvector at  $AOA = 21^\circ$  for the F-15.

Figure 3.8. Magnitude of Eigenvectors at Trigger Point for F-15



The only states that have a magnitude large enough to be seen are  $p$ ,  $\phi$  and  $\beta$ . The vectors show that longitudinal and lateral motion are in fact decoupled. The critical states involved in dutch roll behavior are now  $p$ ,  $\phi$  and  $\beta$ . The magnitude of  $r$  is so small that it can be disregarded. The vectors confirm previous research that dutch roll motion consists of a significant amount of yaw at low AOA and as AOA is increased the motion becomes dominated by rolling motion (19:14). At low angles-of-attack dutch roll is often approximated by a two degree of freedom expression eliminating the roll contribution. In order to examine the motion occurring, as wing rock is triggered the eigenvector structure of the system reveals that only the primary states of  $\beta$ ,  $\phi$ ,  $p$  need remain. Thus a lower order approximate system will be based solely on the following

equations:

$$\begin{aligned} \Delta \dot{\beta} = & \left[ \frac{g}{V_o} \sin(\theta_o + \alpha_o) + \frac{QS}{mV_o} C_{y\beta} \right] \Delta \beta \\ & + \left[ \frac{QS}{mV_o} C_{y_p} + \sin \alpha_o \right] \Delta p + \frac{g}{V_o} \cos \theta_o \Delta \phi \end{aligned} \quad (3.10)$$

$$\Delta \dot{p} = A(C_{L_\beta} + BC_{N_\beta}) \Delta \beta + A(C_{L_p} + BC_{N_p}) \Delta p \quad (3.11)$$

$$\Delta \dot{\phi} = \Delta p \quad (3.12)$$

### Characteristic Equation

In order to study the triggering of wing rock the characteristic equation of the new approximate state matrix must be determined. The new matrix is

$$\begin{bmatrix} \left[ \frac{g}{V_o} \sin(\theta_o + \alpha_o) + \frac{QS}{mV_o} C_{y\beta} \right] & \frac{QS}{mV_o} C_{y_p} + \sin \alpha_o & \frac{g}{V_o} \cos \theta_o \\ A(C_{L_\beta} + BC_{N_\beta}) & A(C_{L_p} + BC_{N_p}) & 0.0 \\ 0.0 & 1 & 0.0 \end{bmatrix} \quad (3.13)$$

The characteristic equation of the above matrix is shown below in expanded polynomial form. The spiral mode has been eliminated from this approximation.

$$\begin{aligned} s^3 - & \left[ \frac{g}{V_o} \sin(\theta_o + \alpha_o) + \frac{QS}{mV_o} C_{y\beta} + A(C_{L_p} + BC_{N_p}) \right] s^2 \\ & + \left[ A(C_{L_p} + BC_{N_p}) \left[ \frac{g}{V_o} \sin(\theta_o + \alpha_o) + \frac{QS}{mV_o} C_{y\beta} \right] - A(C_{L_\beta} + BC_{N_\beta}) \left( \frac{QS}{mV_o} C_{y_p} + \sin \alpha_o \right) \right] s \\ & - \frac{g}{V_o} A(C_{L_\beta} + BC_{N_\beta}) \cos \theta_o = 0 \end{aligned} \quad (3.14)$$

The expression itself looks fairly complicated and examining it does not reveal anything immediately. Upon examining equation 3.6 closely equation 3.14 may be further simplified. For fighter type aircraft most of the mass is concentrated along the aircraft's x-axis. This mass distribution leads to a relatively small resistance to rotation about the x-axis. Three products of inertia  $I_{xy}$ ,  $I_{yz}$ , and  $I_{xz}$  appear in the aircraft equations of motion for a rigid aircraft. By virtue of symmetry,  $I_{xy}$  and  $I_{yz}$  are both equal to zero.  $I_{xz}$  on the other hand in most cases is not zero.  $I_{xz}$  can be thought of as the measure of the uniformity of mass distribution about the x-axis. The axis about which  $I_{xz}$  is equal to zero is defined as the principle inertia axis, and the mass of the aircraft can be considered to be concentrated on this axis. The inertia axis rarely is coincident with the aircraft centerline therefore, the  $I_{xz}$  parameter cannot be set to zero. However, for fighter type aircraft this term is relatively small when compared to the  $I_z$  and  $I_y$  terms. The following figure shows how mass is distributed in a fighter type aircraft.

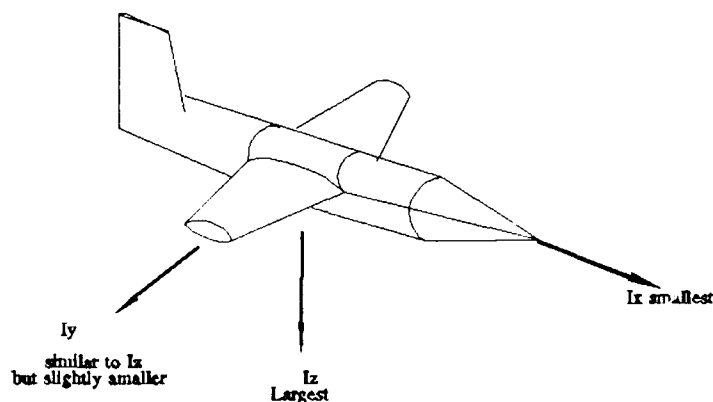


Figure 3.9. Fighter Mass Distribution

$I_{xz}$  is normally two orders of magnitude smaller than  $I_y$  and  $I_z$ . Therefore, the  $I_{xz}/I_z$  term

is small in comparison to one. The same is true of the  $I_{xz}^2/I_x I_z$  term in the variable A.

Thus A may now be represented by

$$A = \frac{QSb}{I_x} \quad (3.15)$$

and the terms multiplied by B can be disregarded due to their relative size. Appendix

D contains inertia data for some representative fighter aircraft. The polynomial is now

$$\begin{aligned} & s^3 - \left[ \frac{g}{V_o} \sin(\theta_o + \alpha_o) + \frac{QS}{mV_o} C_{y_\beta} + AC_{l_p} \right] s^2 \\ & + \left[ AC_{l_p} \left[ \frac{g}{V_o} \sin(\theta_o + \alpha_o) + \frac{QS}{mV_o} C_{y_\beta} \right] - AC_{l_\beta} \left( \frac{QS}{mV_o} C_{y_p} + \sin \alpha_o \right) \right] s \\ & - AC_{l_\beta} \frac{g}{V_o} \cos \theta_o = 0 \end{aligned} \quad (3.16)$$

The dutch roll mode is sitting on the imaginary axis at the trigger point. Therefore, at this point it becomes convenient to view the polynomial in the frequency domain. At the trigger point the real portion of s is zero so s can be replaced by i $\omega$ . Rewriting the polynomial in simpler form the expression becomes

$$A_1 s^3 - A_2 s^2 + A_3 s - A_4 = 0 \quad (3.17)$$

now substituting  $s = i\omega$

$$-A_1 i \omega^3 + A_2 \omega^2 + A_3 i \omega - A_4 = 0 \quad (3.18)$$

grouping the real and imaginary parts yields

$$(+A_2 \omega^2 - A_4) + (-A_1 \omega^3 + A_3 \omega)i = 0 \quad (3.19)$$

Each portion of equation 3.19 must equal zero for the equality to hold. This results in two equalities

$$+A_2 \omega^2 - A_4 = 0 \quad (3.20)$$

$$-A_1 \omega^3 + A_3 \omega = 0 \quad (3.21)$$

The wing rock motion occurs at a frequency other than zero so an  $\omega$  may be factored from equation 3.21 yielding

$$-A_1 \omega^2 + A_3 = 0 \quad (3.22)$$

Multiplying equation 3.20 by  $A_1$  and equation 3.22 by  $A_2$  and subsequently adding the expressions will remove frequency dependence and produce

$$A_2 A_3 - A_1 A_4 = 0 \quad (3.23)$$

When equation 3.23 is satisfied wing rock is triggered. The coefficients are

$$\begin{aligned} A_1 &= 1 \\ A_2 &= \left[ \frac{g}{V_o} \sin(\theta_o + \alpha_o) + \frac{QS}{mV_o} C_{y\beta} + AC_{l_p} \right] \\ A_3 &= AC_{l_p} \left[ \frac{g}{V_o} \sin(\theta_o + \alpha_o) + \frac{QS}{mV_o} C_{y\beta} \right] - AC_{l_\beta} \left[ \frac{QS}{mV_o} C_{y_p} + \sin \alpha_o \right] \\ A_4 &= AC_{l_\beta} \frac{g}{V_o} \cos \theta_o \end{aligned} \quad (3.24)$$

Equation 3.23 will be labeled  $X_\phi$ . Thus when  $X_\phi$  is zero wing rock is triggered.

The expanded expression for the trigger parameter  $X_\phi$  is

$$\begin{aligned} X_\phi &= \left[ \frac{g}{V_o} \sin(\theta_o + \alpha_o) + \frac{QS}{mV_o} C_{y\beta} + AC_{l_p} \right] \\ &\quad \left[ AC_{l_p} \left[ \frac{g}{V_o} \sin(\theta_o + \alpha_o) + \frac{QS}{mV_o} C_{y\beta} \right] - AC_{l_\beta} \left[ \frac{QS}{mV_o} C_{y_p} + \sin \alpha_o \right] \right] \\ &\quad - (AC_{l_\beta} \frac{g}{V_o} \cos \theta_o) \end{aligned} \quad (3.25)$$

### Validation of Expression

The goal of this study is to be able to predict wing rock without using complicated software such as the AUTO routine. Thus, the trigger point should vanish at the trigger point predicted by AUTO. AUTO has provided the state values at the critical solution

point and the inertia data for the Eagle is shown in Appendix A. Using this information,  $X_\phi$  has been calculated over the angle-of-attack range of interest. This data is presented in Table 3.5.

Table 3.5. Wing Rock Parameter and Coefficient Values for the F-15

Alpha (degrees)	A2	A3	A4	$X_\phi$
10	.66	2.36	.87	.69
15	.44	2.98	1.10	.22
20	.32	3.06	.98	.005
25	.18	2.01	.58	-.21
30	.13	1.80	.54	-.31

As can be seen in Table 3.5 the trigger parameter is monotonically decreasing and the value of the trigger parameter crosses through zero near  $20^\circ$ . Here the trigger predicts wing rock onset at an angle-of-attack of slightly greater than  $20^\circ$ . The bifurcation predicted angle-of-attack for wing rock onset was  $21^\circ$ . Hence, the data provided by bifurcation analysis verifies equation 3.25. Figure 3.10 shows the trigger parameter versus angle-of-attack.

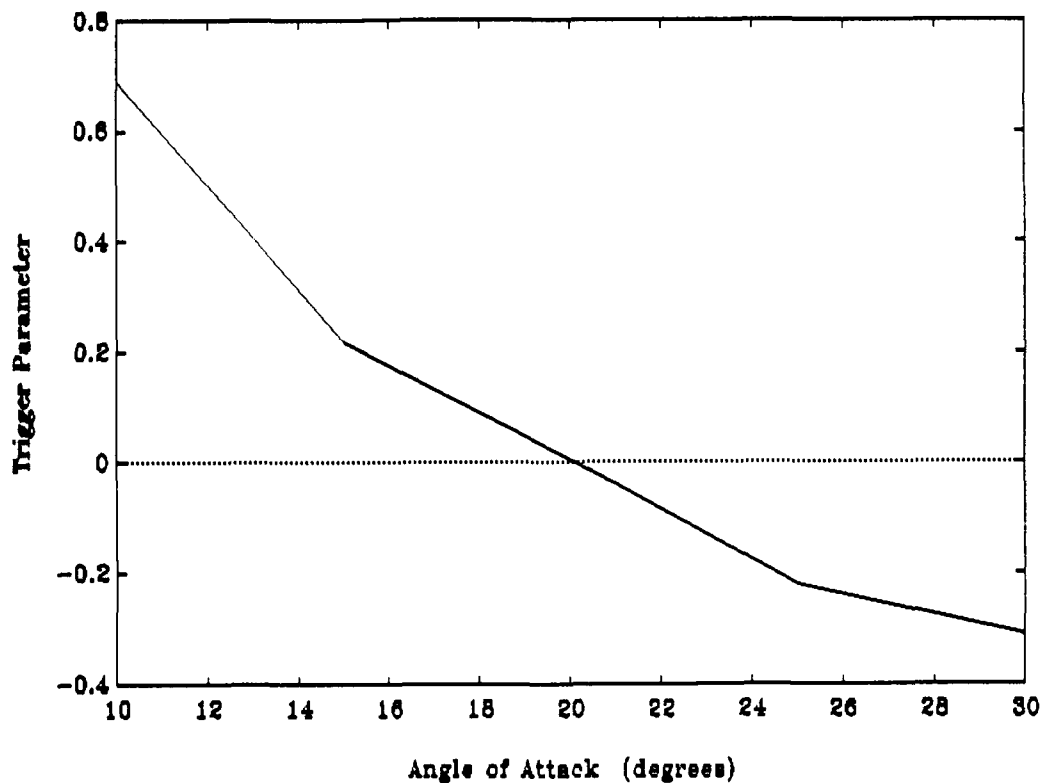


Figure 3.10. Trigger Parameter Versus Angle-of-Attack for F-15

#### Prediction Procedure

One of the objectives of this study is to develop a relatively simple method to predict

wing rock. Given the aircraft stability derivatives, inertia data and physical characteristics we should be able to predict the AOA at which an aircraft will wing rock using the following iterative procedure. The following is based on an aircraft operating at an equilibrium condition.

---

1. The first step in this process is to choose an angle-of-attack as an initial starting point. This step will provide  $\alpha_o$ .
2. At an equilibrium condition the moment coefficient will equal zero. Therefore, with  $C_m = 0$  and  $C_m(\alpha_o, \delta e_o)$  the elevator deflection can be found.
3. Combining the following equations the initial pitch angle can be found (16:258).

$$mg \sin \theta_o = C_{x_o} \frac{1}{2} \rho V_o^2 S \quad (3.28)$$

$$-mg \cos \theta_o = C_{z_o} \frac{1}{2} \rho V_o^2 S \quad (3.29)$$

with

$$C_{x_o} = f(\alpha_o, \delta e_o) \quad (3.30)$$

$$C_{z_o} = f(\alpha_o, \delta e_o) \quad (3.31)$$

yields

$$\theta_o = \tan^{-1} \left( \frac{C_{x_o}}{C_{z_o}} \right) \quad (3.32)$$

4. With the initial angle-of-attack, pitch angle and elevator deflection equation 3.28 can be rewritten to solve for  $V_o$ .

$$V_o = \left[ \frac{2mg \sin \theta_o}{C_{X_o} \rho S} \right]^{\frac{1}{2}} \quad (3.33)$$

5. There is now enough information to compute  $X_o$  from equation 3.25.
6. Repeat steps 1 through 5 until the angle where  $X_o$  equals zero is found. A sign change in the triggering parameter would indicate that the step size is too big and the critical angle has already been exceeded.
7. The frequency at which wing rock occurs can be found from the following expression

$$\omega = \left[ \frac{A_4}{A_2} \right]^{\frac{1}{2}} \quad (3.34)$$

where  $A_4$  and  $A_2$  are specified in equation 3.24.

---

The above procedure should provide a reasonable estimate of the state variables at the aircraft's specific trigger point and the initial frequency of the wing rock motion.

### Critical Stability Derivatives

A quick inspection of equation 3.25 reveals that four stability derivatives are critical to predicting the onset of wing rock. These derivatives are  $C_{yp}$ , side force due to roll rate,  $C_{y\beta}$ , side force due to sideslip,  $C_{lp}$ , roll damping, and  $C_{l\beta}$ , rolling moment due to sideslip.

The contribution of  $C_{yp}$  to the trigger parameter is in fact small. The sideforce due to roll rate parameter is normally two orders of magnitude smaller than the sine of the equilibrium angle-of-attack and for many modern configurations  $C_{yp}$  is zero (23:628). Therefore,  $C_{yp}$  has little or no effect on the actual value of the trigger parameter and its

contribution can be neglected.

$C_{y\beta}$ , the sideforce due to sideslip, provides a small contribution to the  $A_2$  coefficient in the trigger parameter expression. This contribution is one order of magnitude smaller than the contribution of the roll moment due to sideslip. While the derivative is large enough to be considered its contribution does not require any significant analysis.

The findings of this study agree with the findings of Johnston (11). The critical stability derivatives contributing to the onset of wing rock are  $C_{l_p}$ , roll damping, and  $C_{l\beta}$ , roll moment due to sideslip.

The following equation

$$C_l = C_{l_\beta} \beta + C_{l_{\delta_a}} \delta_a \quad (3.35)$$

shows that an aileron deflection produces a rolling moment and thus the aircraft will accelerate in roll. During a steady state roll, sideslip is kept near zero and thus its effects can be considered negligible. Thus, by inspection of equation 3.35 it would appear that for a constant aileron deflection a constant rolling moment would result. This moment should produce a continually increasing roll rate. Since this is not the case there must be something which opposes the rolling motion. When an aircraft is given a rolling velocity to the right, the right wing (downgoing) experiences an increase in  $\alpha$  due to the helix angle of roll (12:251) and the left (upgoing) wing experiences a decrease in  $\alpha$ . Thus the downgoing wing experiences an increase in lift and the upgoing wing experiences a decrease in lift (for angles-of-attack less than that for maximum lift) and a rolling moment is developed that opposes the rolling motion. This moment is roll

damping and it is attributed to the roll damping stability derivative  $C_{l_p}$ . Thus a better equation for roll moment would be

$$C_l = C_{l_\beta} \beta + C_{l_p} p + C_{l_{\delta_a}} \delta_a \quad (3.36)$$

thus  $C_{l_p}$  must be negative (right roll positive) to produce a steady state roll rate.

$C_{l_p}$  is a function of wing sweep, aspect ratio and the wing's lift curve slope. An aircraft with a straight, highly efficient, high aspect ratio wing would have a large negative value of  $C_{l_p}$  and hence would exhibit high roll damping. Thus, a fighter aircraft with highly swept, thin, low aspect ratio wings would exhibit poor roll damping. Any roll motion the aircraft exhibits will be countered by this derivative.

$C_{l_\beta}$  is often referred to as the lateral stability or dihedral effect derivative. This derivative relates an aircraft's ability to produce a rolling moment due to a sideslip angle. For positive lateral stability a positive sideslip should result in a rolling moment to the left, this results in a negative  $C_{l_\beta}$  for lateral stability. The number one contributor to  $C_{l_\beta}$  is an aircraft's wing. Wing sweep, wing dihedral, wing position and the wing's ability to produce lift all greatly effect  $C_{l_\beta}$ . An increase in wing sweep, wing dihedral and  $C_{l_\alpha}$  will all produce a corresponding increase in the magnitude of  $C_{l_\beta}$  (23:261). The second largest contributor to  $C_{l_\beta}$  is the vertical tail, because the lift force created on the tail by a sideslip angle produces a moment about the roll axis. A conventional vertical tail has a stabilizing effect on  $C_{l_\beta}$ .

Previous research has shown that  $C_{l\dot{\beta}}$  is directly related to dutch roll damping and therefore to wing rock motion (19:14). Small magnitudes of  $C_{l\dot{\beta}}$  result in dutch roll motion that is highly damped and characterized by mostly yaw and sideslip. This type of motion is characteristic of a straight wing aircraft with negative or no dihedral angle. Fighter aircraft on the other hand, with highly swept wings, exhibit large magnitude dihedral effect derivatives that result in poorly damped dutch roll motion that consists of little yaw and sideslip and a majority of roll. Roskam (23:261) has shown that a negative increase in  $C_{l\dot{\beta}}$  results in a corresponding decrease in dutch roll damping.

From the above description of the two critical derivatives it appears that  $C_{l\dot{\beta}}$  and  $C_{l\dot{p}}$  are in conflict with each other and in fact that is the case. Both derivatives have the same response to an increase in wing efficiency (lift curve slope). However, the most critical wing characteristics appear to be sweep, aspect ratio and dihedral angle. Thus, disregarding lift curve slope, the characteristics that would result in a larger  $C_{l\dot{p}}$  would produce a smaller  $C_{l\dot{\beta}}$ . This would be fine if the aircraft in question was a transport requiring a large straight wing planform. The wing characteristics which give a fighter aircraft its increased performance also produce wing rock. A fighter aircraft with a highly swept wing designed to produce large roll rates will have a larger negative value  $C_{l\dot{\beta}}$  and a smaller negative value of  $C_{l\dot{p}}$ . Equation 3.25 thus makes sense as far as this conflicting relationship between dihedral effect and roll damping is concerned. Therefore, a fighter aircraft which possess a small negative value of  $C_{l\dot{p}}$  and a relatively large value of  $C_{l\dot{\beta}}$  will have a greater tendency to exhibit wing rock characteristics.

These findings agree with the open-loop critical departure parameters studied by Johnston (11:3).

## IV. Application of Analytical Results

In order to verify the results of chapter three the procedure developed was applied to an existing fighter aircraft. Data was taken from an extensive high AOA study involving the F-4 Phantom and the F-14 Tomcat. This investigation was conducted by Systems Technology, Inc. and was sponsored by the Air Force Flight Dynamics Laboratory at Wright-Patterson Air Force Base.

The F-4 data from the above study was used to verify the triggering parameter expression (equation 3.25) and the wing rock frequency expression (equation 3.34) developed in Chapter 3.

The physical characteristics of the F-4J are contained in Appendix B. The important state values, the trigger parameter and the trigger parameter coefficients are shown in table 4.1.

Table 4.1 Trigger Parameter and Coefficient values for F-4J

Alpha	Pitch	Velocity	A2	A3	A4	X $\phi$
10	15	347	.638	3.05	1.21	.74
15	15.2	271	.408	2.88	.93	.24
20	13.5	260	.205	1.95	.49	-.089
25	10	245	-.003	1.01	.19	-.193

The angles in table 4.1 are in degrees while the velocity is in feet per second. Figure 4.1 is a plot of angle-of-attack versus the trigger parameter for the F-4J.

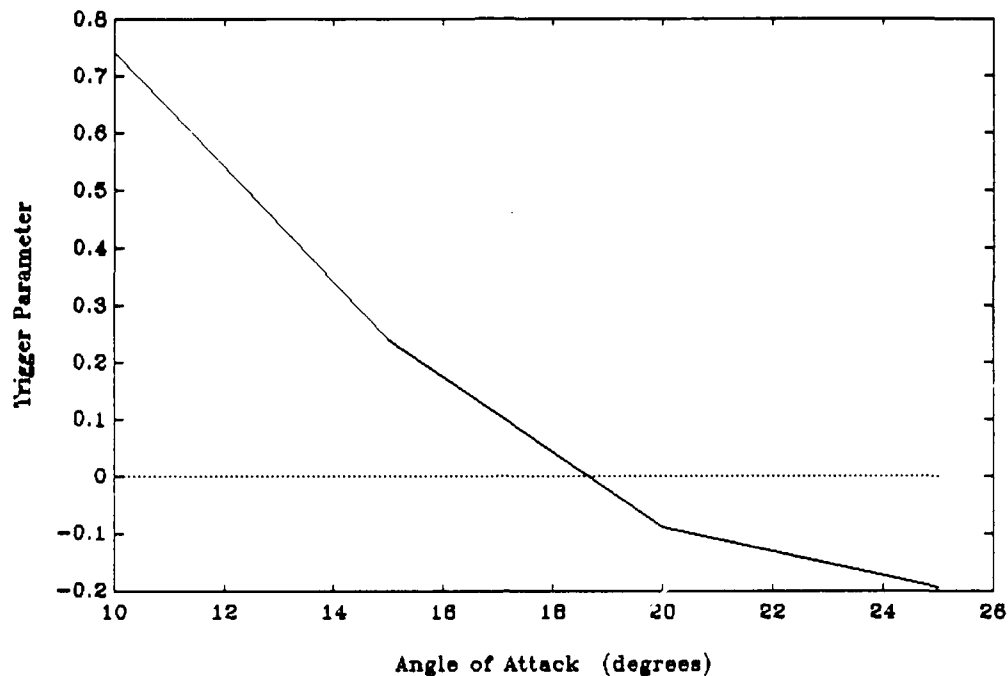


Figure 4.1. AOA vs Trigger Parameter For F-4J

Figure 4.1 shows that the trigger parameter passes through zero at  $18.5^\circ$  angle-of-attack, thus predicting wing rock at  $18.5^\circ$  AOA. This is within  $.5^\circ$  of the flight test data agrees presented in the referenced high angle-of-attack study (test data shows  $19^\circ$ ). Figure 4.2 shows the F-4 trimmed lift curve which illustrates the basic high angle-of-attack behavior of the Phantom.

The frequency predicted by equation 3.34 for wing rock at its onset is 1.5 cycles per second. Flight test data shows that the actual frequency is 1.2 cycles per second.

Overall, the F-4 data contained in the referenced high angle-of-attack study (11) confirmed the results of Chapter 3.

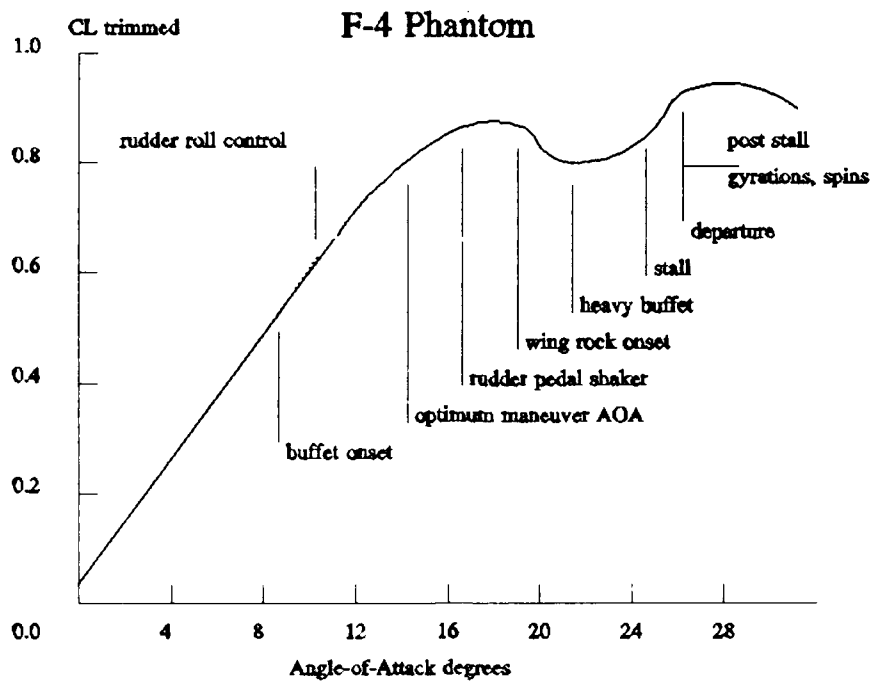


Figure 4.2. F-4 Trimmed Lift Curve (11:6)

## V. Flight Test Method

The flight test portion of this project was conducted as a USAF Test Pilot School Staff project. The test team consisted of various members of the Test Pilot School Staff. The project pilots were all graduates of the USAF TPS or the USN TPS.

The test team flew eight sorties totaling 8.8 flight hours between 15 March and 1 May 1992 at the Air Force Flight Test Center (AFFTC), Edwards Air Force Base California. The flight test consisted of four aircraft sorties each in the RF-4C and the T-38A.

### Test Item Description

A basic description of production representative F-4 and T-38 aircraft has been presented in Chapter 2. The following information highlights the differences between the standard operational models and the aircraft used in testing.

The RF-4C aircraft used in this test was production model 65-850. This aircraft is one of two remaining flight test instrumented F-4 aircraft at the Flight Test Center. This aircraft has been modified with the USAF TPS Data Acquisition System (DAS). This installation allows real-time data acquisition by suitably equipped ground stations. A modified main instrument panel has been installed in the aircraft's front cockpit to accommodate this system. This panel contains system power switches and new flight instruments which include: angle-of-sideslip, aileron position, stabilizer position, rudder position, sensitive airspeed indicator and sensitive accelerometer. A magnetic tape

recorder and a recorder control head have also been installed in the rear cockpit of the RF-4C. This airborne recording system is capable of recording 40 separate data parameters as well as aircrew verbal comments. The tapes used by this system are capable of recording up to 2 hours of flight test information. Various transducers have been added to the aircraft to measure control surface positions, control stick and rudder pedal positions, attitude, acceleration, engine parameters, stick forces, outside air temperature, airspeed and altitude. All of this information is fed through a signal acquisition unit to the magnetic tape recorder and the telemetry transmitter. The RF-4C is equipped with the Aydin-Vector Telemetry transmitter. This system is a 10-Watt, L-band transmitter that uses FM modulation. Data from this transmitter is received real time and recorded real time on magnetic tape and strip charts in one of the Test Pilot School's flight test control rooms. This equipment replaces the aircraft's original tactical reconnaissance system therefore, the test article's mass properties are not altered significantly. The aircraft's DAS samples data eight times a second.

The T-38A flown was production model 68-8154. This aircraft has also been modified with a data acquisition system similar to that described above for the RF-4C. However, the T-38A DAS has been upgraded to a Metraplex system. The Metraplex system allows 38 data parameters to be sampled at 32 times per second. The system records this data, along with cockpit voice on magnetic tape and also has the telemetry capabilities of the RF-4C. This T-38 has also been equipped with angle-of-attack and angle-of-sideslip indicators as well as sensitive airspeed and acceleration indicators. The

aircraft has been fitted with a YAPS nose boom. The YAPS head contains pressure pickups for airspeed and altitude transducers as well as angle of attack and yaw vanes. The aircraft has extensive instrumentation differences from the representative field example T-38A. However, these differences should not have a significant effect on the aircraft's stability characteristics. If the reader has any questions concerning test equipment please consult the appropriate partial flight manual. These documents are listed as references 29 and 31.

### Data Reduction

Quantitative data was collected by two means. Telemetered data was recorded on ground based magnetic tape recorders for post-mission analysis. From these tapes digital listings of aircraft data parameters were derived. These listings were used as the primary data source for post-flight data analysis. Flight parameters were also recorded on airborne magnetic tape and were used as a backup source of information.

Qualitative data was also collected to confirm conclusions drawn from quantitative data analysis. Pilot comments addressing flight test method and wing rock onset characteristics were also recorded.

Data Acquisition System parameters and data resolutions for both aircraft are shown in Appendix E. Parameters recorded at the test point are listed in table 5.1. Those parameters required for data purposes are identified with an "R"; and those desired for completeness of data are identified with a "D".

Table 5.1. Test Parameters

DAS Parameter	Code
Angle of Attack	R
Angle of Sideslip	R
Longitudinal Stick Position	D
Lateral Stick Position	D
Rudder Pedal Position	D
Calibrated Airspeed	R
Mach Number	R
Calibrated Airspeed	D
Pitch Angle	R
Roll Angle	D
Pitch Rate	D
Roll Rate	D
Yaw Rate	D
R = Minimum Required Parameter D = Desired Additional Parameter	

### Test Conditions and Methods

All test flights for this program were conducted in day visual meteorological conditions in restricted airspace (R-2508) operated by the AFFTC, Edwards AFB California.

This study proposes that wing rock onset occurs as the dutch roll mode of an aircraft becomes unstable. In order to decouple the longitudinal and lateral characteristics involved with triggering this instability, a 1-g stall approach was used. Critical data at the onset point includes  $\alpha$ ,  $\beta$ ,  $p$ ,  $q$ ,  $r$ ,  $\theta$ ,  $\phi$  and  $V$ . This test maneuver was a near stall investigation in both aircraft. However, the T-38 was permitted to enter a full aft stick stall. The specific flight test technique used to gather the wing rock onset data is

outlined in the following paragraph.

Each test aircraft was in a clean configuration for this maneuver (gear, flaps and speed brake retracted, with no external stores). The test aircraft were trimmed at 20,000 ft pressure altitude and .6 Mach. Throttles were then placed at 80% for the RF-4C and 85% for the T-38A and altitude was maintained until 250 KCAS. At 250 KCAS the aircraft pitch attitude was adjusted to hold a 1 kt/sec bleed rate. For the RF-4C, this bleed rate was held until 25° AOA, nose rise, nose slice or  $\pm 30^\circ$  of wing rock, whichever occurred first. For the T-38A, this bleed rate was held until full aft stick was achieved. The aircraft control stick was centered to prevent lateral inputs. The rudder was also held in the neutral position to prevent lateral or directional inputs.

In the interest of flight safety and data accuracy the following test limitations were observed:

1. Testing was accomplished at 20,000  $\pm$  200 ft pressure altitude.
2. Test aircraft were operated in accordance with the applicable aircraft flight manual.
3. No abrupt throttle movements were made during testing.
4. The F-4 was limited to 25° AOA, nose rise, nose slice or  $\pm 30^\circ$  of wing rock whichever occurred first.
5. There were no aggravated inputs performed during test maneuvers.
6. Applicable aircraft departure recovery procedures were briefed before each flight.
7. If aircraft departure occurred, flight manual recovery procedures were initiated and the test point terminated until the cause of the departure was determined.
8. The RF-4C test maneuver was conducted with the roll augmentation turned off.
9. The T-38A test maneuver was conducted with the yaw augmentation turned off.

The test points are well within the established flight envelopes of the RF-4C and the T-38A. The test points are listed in table 5.2.

Table 5.2. Test Point Summary

Test Point	Trim Condition	Maneuver	G Loading	Bleed Rate kt/sec	Remarks
Point 1 RF-4C	20,000ft M=0.6	1 G Stall	1	1	Roll Aug Off
Point 1 T-38A	20,000ft M=0.6	1 G Stall	1	1	Yaw Aug Off

Prior to each test sortie the test team members were asked to record their qualitative observations regarding wing rock. The pilots were requested to record angle-of-attack and roll angle data while the rear seat crew members were asked to look for any pitch and yaw oscillations accompanying the rolling motion.

## VI. Flight Test Results

Due to operational constraints and aircraft availability eight dedicated test sorties were not conducted. Two 1-G stalls were accomplished on each of eight sorties that also supported TPS instructor training. The first stall was used to practice the flight test technique and check the test instrumentation while the second stall was used for gathering the test data. If the DAS was found inoperative on the first stall the second stall was accomplished and hand held data was recorded. T-38 flight testing continued until 1 May 1992. RF-4C flight testing was completed 9 April 1992.

### T-38A Flight Test Results

Data Analysis. Four data sorties were conducted in the T-38A. A DAS failure occurred on sortie number 2. The only information recorded on this flight were pilot comments and flight engineer hand held data. The qualitative data obtained on the second sortie was used in conjunction with the DAS data from the remaining flights to validate the analytical findings of Chapter 3.

Prior to actual flight testing the prediction procedures outlined in Chapter 3 were accomplished using data for the T-38A. For these calculations the aircraft weight was assumed to be 12,000 LBS, the wing area was 170 sq ft and the wing span was 25.25 ft. The following table shows the results obtained at three representative angle-of-attack values. In this case angle-of-attack, pitch angle and velocity are the trim values

determined by the prediction procedure.  $Q$  represents the dynamic pressure and  $A$  is the value determined by equation 3.15. The stability derivatives were obtained from Northrop wind tunnel data (8). The remaining parameters in table 6.1 were derived directly from the prediction procedure (The Frequency prediction will be discussed later in Chapter 6).

Table 6.1. Predicted Trigger Parameter Values T-38A

Alpha	5	10	15	degrees
Pitch	7	6.7	5.8	degrees
Velocity	399	296	239	ft/sec
$Q$	100	55.1	35.9	lbs/ft <sup>2</sup>
$A$	286	157	103	/sec <sup>2</sup>
$C_{l\beta}$	-.00125	-.002	-.002	/deg
$C_{lp}$	-.31	-.25	-.08	/rad
$C_{y\beta}$	-.02	-.02	-.018	/deg
$A_2$	1.535	0.659	0.097	
$A_3$	1.761	3.106	3.050	
$A_4$	1.640	1.930	1.480	
$X\phi$	1.064	0.117	-1.180	

This data was calculated over the known operating range for the T-38A. The T-38A cruises at approximately 5° AOA and the aircraft will be fully stalled, with full back stick, at roughly 15° AOA. Table 6.1 shows that as alpha is increased the aircraft dihedral effect increases as the roll damping decreases. Johnston (11) has previously shown these characteristics to be ideal for wing rock development. The side force due

to sideslip remains essentially unchanged. The following figure shows the predicted trigger parameter plotted against angle-of-attack for the T-38A.

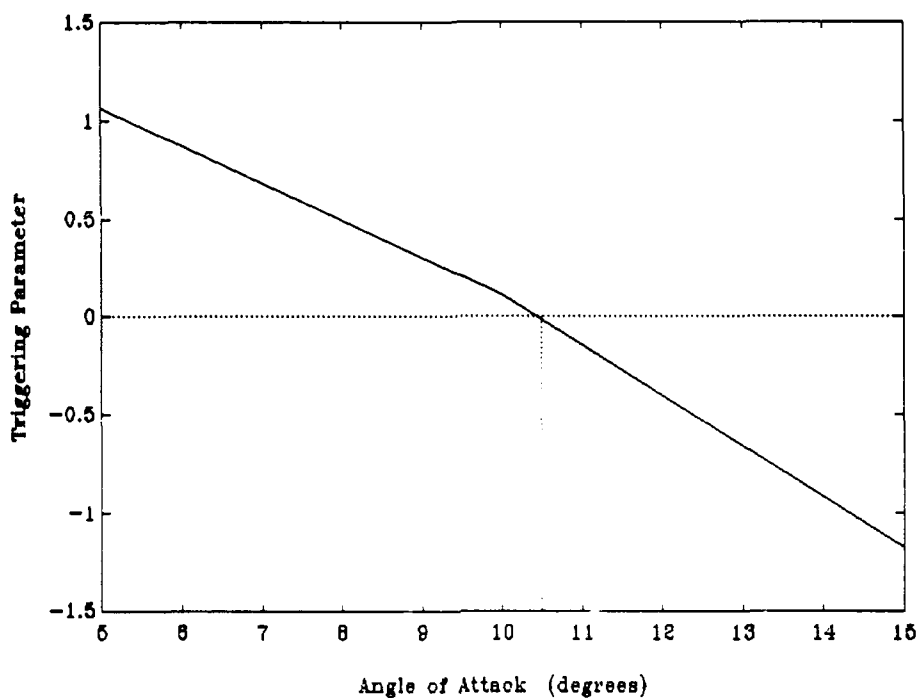


Figure 6.1. T-38A Wing Rock Prediction

This plot shows that the trigger parameter goes to zero at approximately  $10.5^\circ$ . If the development of the triggering parameter is correct T-38A wing rock onset should occur at  $10.5^\circ$  during a 1-G approach to stall flight condition.

Due to the departure characteristics of the T-38, flight testing was terminated at the discretion of the test pilot (as an advanced trainer the T-38 exhibits excellent stall characteristics and is extremely difficult to depart). Maneuver termination usually occurred shortly after the development of a full aft stick stall. The following table summarizes the critical parameters obtained at wing rock onset during flight test maneuvering of the T-38A.

Table 6.2. Summary of T-38A Flight Test Results

	Date	Airspeed ft/sec	Pitch degrees	Alpha degrees
Flight Number 1	2 Apr 92	295.1	6.7	10.12
Flight Number 2	9 Apr 92	296	7	10*
Flight Number 3	22 Apr 92	296.3	6.6	9.96
Flight Number 4	5 May 92	295.8	6.6	10.00

\* Flight with malfunctioning data acquisition system   # Pilot comment 10 degrees  $\pm$  .5

The flight test results consistently show wing rock onset occurring in the vicinity of 10° AOA for the T-38A for a 1-G approach to stall flight condition. The Metraplex system is only accurate to .5°, while measuring AOA, but the data is very closely spaced for the three sorties that the DAS was functioning properly. 10° AOA appears to be the actual point of wing rock onset for a T-38 approaching a 1-G stall. As a prediction scheme the trigger parameter appears to work fairly well. The following figures show aircraft behavior from the point of wing rock onset until the flight test maneuvering was terminated. The data from flight number 1 was the most complete because the test pilot allowed the wing rock motion to continue one full cycle after he achieved full back stick. Figure 6.2 shows aircraft AOA versus time from wing rock onset; each test pilot achieved full back stick at approximately 6 seconds.

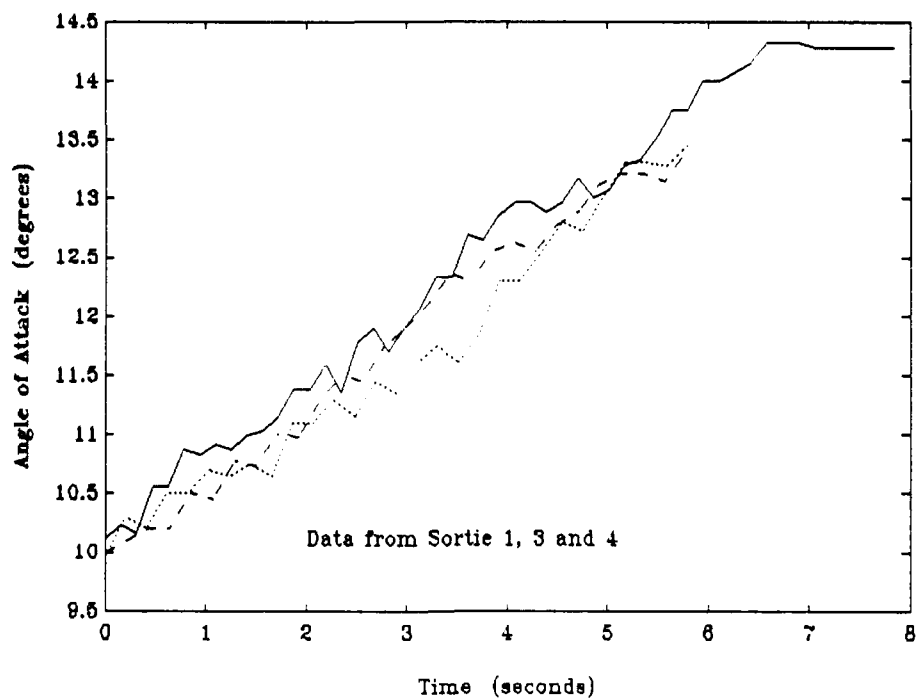


Figure 6.2. AOA vs Time From Wing Rock Onset

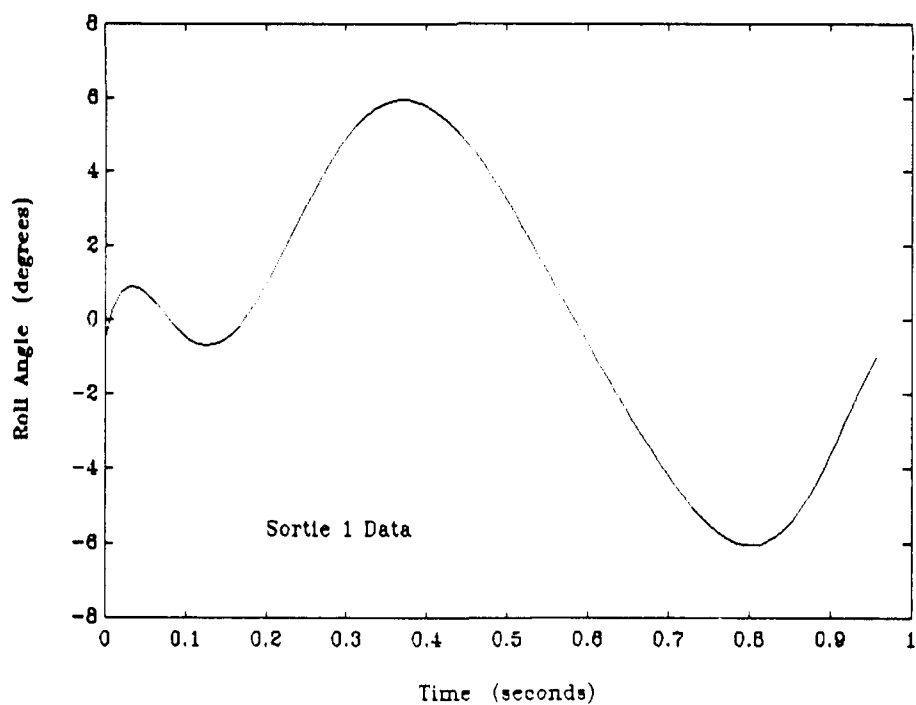


Figure 6.3. Roll Angle 1 Second After Onset

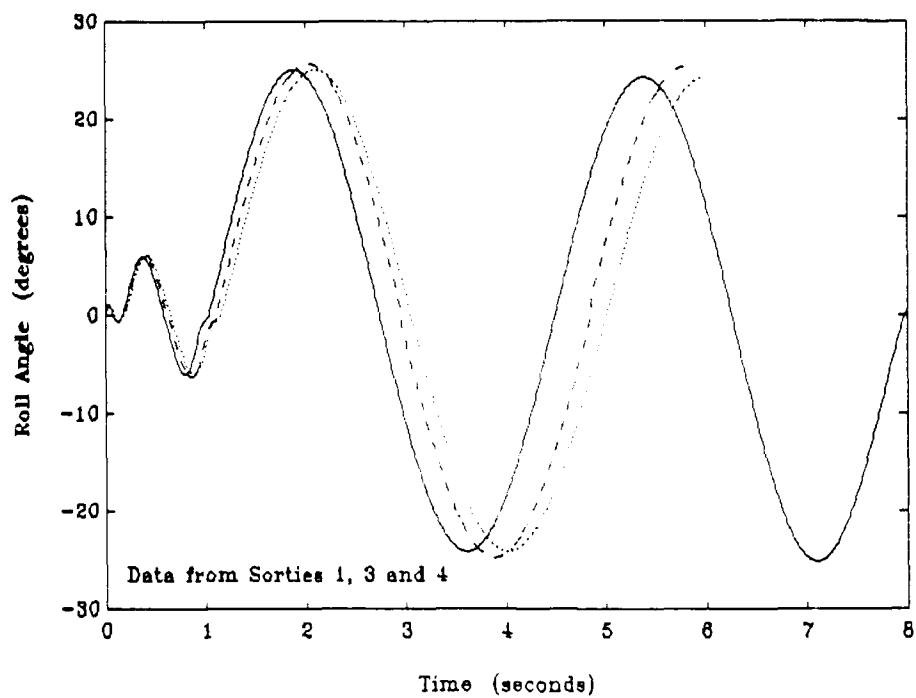


Figure 6.4. Roll Angle vs Time From Onset

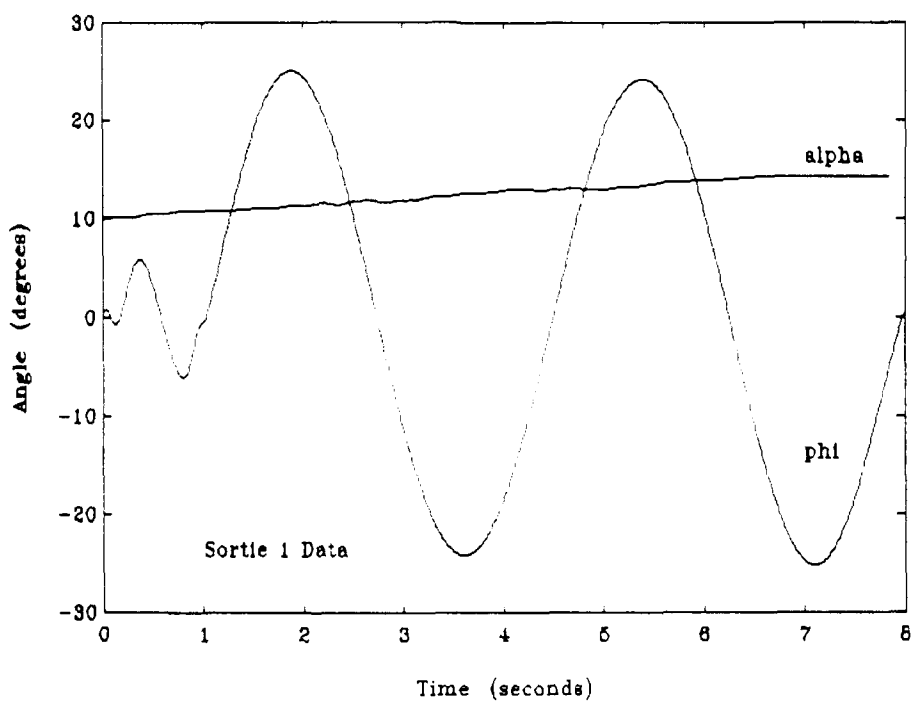


Figure 6.5. Roll Angle and Alpha vs Time T-38A

For the T-38A 1-G stall, AOA grows linearly from wing rock onset until maneuver termination except on sortie 1 where AOA reached a plateau of approximately  $14.3^\circ$ . This plateau was reached as the aircraft entered a fully developed aft stick stall. Figure 6.3 shows the roll angle history during the first second of wing rock during sortie 1. As can be seen the initial roll oscillation is extremely small in magnitude with a frequency of 5 cycles/sec. The frequency prediction parameter (equation 3.34) predicted the initial motion would have a frequency of 1.7 cycles/sec. The T-38 initial motion is much faster than predicted. The first oscillation for the T-38 however, is very small (roll angle magnitude close to  $1^\circ$ ) and is very close to instrumentation tolerances. The second oscillation has a frequency of 1.22 cycles/sec which is much closer to the predicted value. The values predicted by the frequency prediction parameter may be effected by the flight test technique. Due to the limited availability of resources the wing rock onset point was found by constantly increasing angle-of-attack (approach to 1-G stall) without establishing a trim condition at each angle. While this method was effective in identifying wing rock onset, it eliminated the assumptions based on trimmed flight which were used to develop the frequency prediction parameter. Therefore, the frequency prediction parameter may not be a good predictor of the actual motion. Figure 6.4 shows that the initial oscillation is followed by two oscillations with rapidly building magnitude, within 2 seconds of wing rock onset roll angle oscillations were greater than  $25^\circ$ . Roll oscillations on sortie 3 were greatest while the fourth sortie produced the slowest motion. However, the three stalls recorded by the DAS exhibited very similar behavior. The roll angle plot of sortie 1 shows that the growth of the rolling motion

stabilizes within 3 cycles, at this point the rolling motion has approached its limit cycle. For the T-38 the rolling motion is symmetric about the roll axis. Figure 6.5 isolates the AOA and roll angle behavior of sortie 1. Figure 6.6 shows the limit cycle behavior of the T-38A wing rock motion.

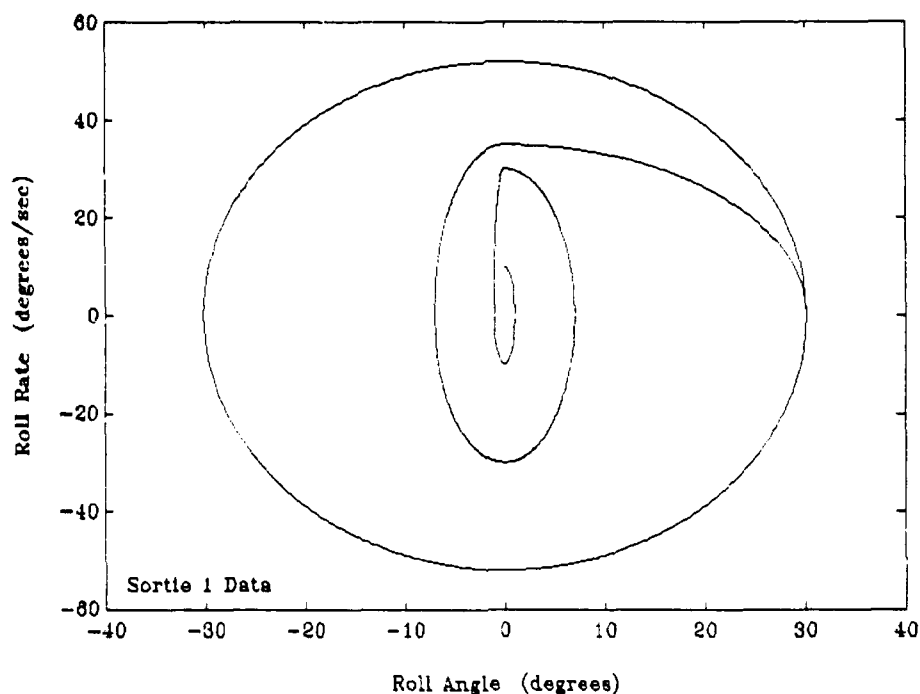


Figure 6.6. T-38A Wing Rock Limit Cycle

The motion starts in the center of the figure and continues to grow outward toward the limit cycle. In this case, a decrease in roll damping accompanies the rolling oscillations at wing rock onset and this decrease continues until the rolling oscillations cause the damping to increase slightly or stop decreasing thus establishing the limit cycle. The symmetric nature of the roll oscillations produces an elliptical growth pattern on the plot of roll angle versus roll rate. For the T-38A the unstable motion occurring at wing rock onset involved almost all roll motion (sideslip magnitude did not exceed  $0.7^\circ$ ). Because

of limited sideslip it appears that the aircraft was nearly rolling about the aircraft's velocity vector. As the bifurcation model predicted with the F-15B (see chapter 3) unstable dutch roll motion at high angles-of-attack involves mostly a rolling motion. This motion is wing rock.

T-38 Test Crew Comments. Four test pilots participated in the T-38A flight test phase. On each sortie the rear seat test pilot acted as the flight test engineer. The flight debriefing and cockpit voice recorded on magnetic tape were used to obtain qualitative observations regarding wing rock behavior in the T-38A. Prior to each flight, the front seat pilot was asked to comment upon the appropriateness of the flight test maneuver versus the data required, the angle-of-attack of wing rock onset and the characteristics of the rolling oscillations occurring during wing rock. All of the front seat pilots commented that wing rock was triggered "at approximately  $10^\circ$  AOA" and that the rolling oscillations very quickly grew to roughly  $\pm 30^\circ$  of bank angle. The test pilot from sortie 1 stated that the aircraft had entered a full aft stick stall with the rolling oscillations stabilized at  $\pm 25^\circ$  of roll. Each front seat pilot felt that the practice maneuver was a good test technique and that it helped to prevent lateral stick inputs during the actual data runs.

The test pilots that occupied the T-38A back seats during these flights were asked to comment on the general nature of the wing rock motion and to specifically attempt to observe aircraft pitch and yaw oscillations once wing rock onset had occurred. The rear seat pilot on sortie 1 stated that the roll oscillations were very fast and that because of their increasing magnitude it was very difficult to see any pitch or yaw changes. The

acting flight test engineer from sortie 3 felt that no pitch or yaw oscillations occurred during the wing rock motion and that he believed that the aircraft was "rolling around a point". DAS data showed the aircraft sideslip angle never exceeded  $0.7^\circ$  and pitch increased and decreased with AOA.

### RF-4C Flight Test Results

Data Analysis. Four data sorties were conducted in the RF-4C. The flights occurred without incident however, due to instrumentation problems roll angle and roll rate information were not collected on the second sortie and pilot voice and flight test engineer hand held data were the only information collected on the fourth sortie. The data collected on the first and third flights was sufficient to validate the findings of Chapter 3 when combined with the qualitative observations of flights two and four.

As with the T-38A, prior to actual flight testing the procedures outlined in Chapter 3 for predicting the onset of wing rock were accomplished using data for the RF-4C.

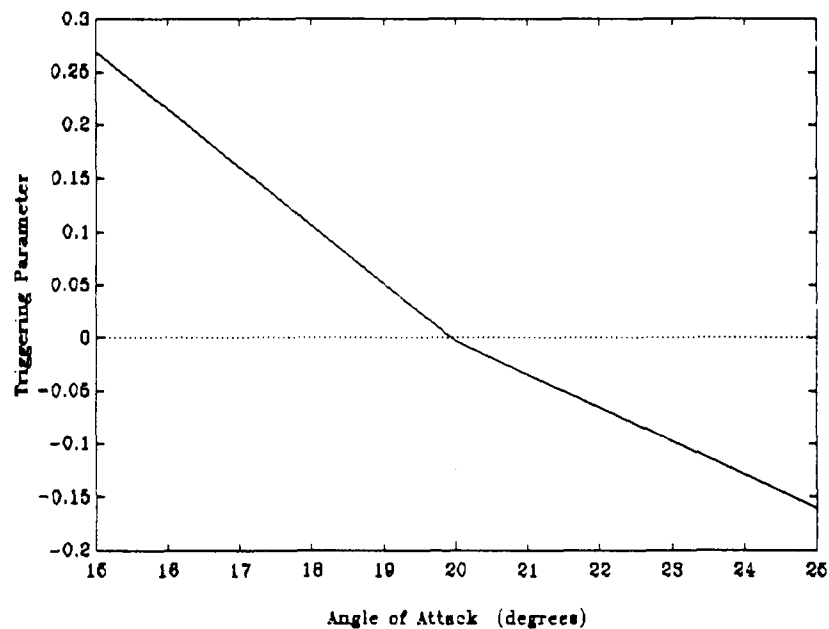


Figure 6.7. RF-4C Wing Rock Prediction

Predicted data was only calculated for the AOA range of interest of 15 to 25 degrees. Due to the departure characteristics of the RF-4C, flight testing was not permitted above 25° AOA. The RF-4C is departure prone above 25° AOA. In an attempt to limit risk, both to aircraft and aircrew, RF-4C maneuvering was terminated a 25° AOA. Figure 6.1 shows the trigger parameter plotted versus angle-of-attack. This plot shows that the triggering parameter goes to zero at a value slightly less than 20° AOA. Therefore, if prior analysis is correct wing rock onset should occur in the vicinity of 20° AOA for the RF-4C in a 1-G approach to stall.

The following table summarizes the critical parameters obtained at wing rock onset during the flight test maneuver for the RF-4C.

Table 6.3. Summary of RF-4C Flight Test Results

	Date	Airspeed ft/sec	Pitch degrees	Alpha degrees
Flight Number 1	15 Mar 92	274.1	13.5	19.85
Flight Number 2	17 Mar 92	273	15	20
Flight Number 3	1 Apr 92	274.3	13.2	19.71
Flight Number 4	9 Apr 92	276	15	20

\* Flights with malfunctioning data acquisition systems

The results consistently show wing rock being triggered near 20° AOA in a 1-g stall.

Even though DAS data was not collected on sorties 2 and 4, test pilot observations and

flight test engineer hand held data place the wing rock onset point at  $20^{\circ}$  AOA for both flights. The data acquisition system was slightly more accurate at identifying this point. Wing rock was triggered at  $19.85^{\circ}$  on the first sortie while onset occurred at  $19.71^{\circ}$  on the third sortie. The Aydin-Vector DAS system has a data resolution of  $.273^{\circ}$  for angle-of-attack measurements. Therefore, the actual wing rock onset point could lie within a  $.273^{\circ}$  neighborhood of the shown value. Much like the T-38A data, the RF-4C data is very closely spaced and thus assumed accurate. As a prediction tool the triggering parameter appears to be providing a fairly accurate estimate of the angle-of-attack at wing rock onset for the RF-4C.

The following figures show AOA and roll angle magnitude data for the eight seconds following wing rock onset.

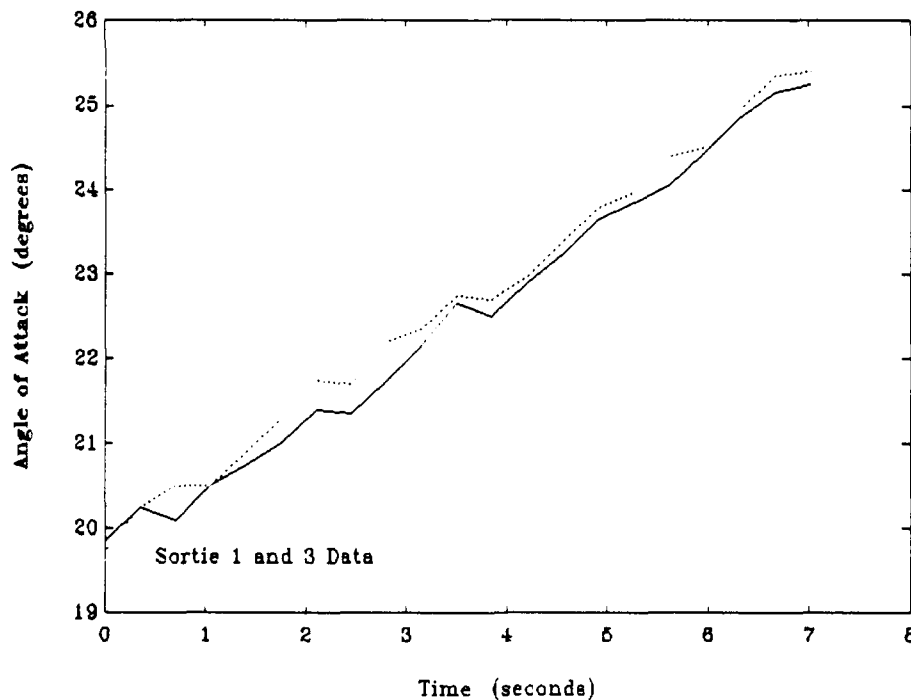


Figure 6.8. Angle of Attack vs Time From Wing Rock Onset

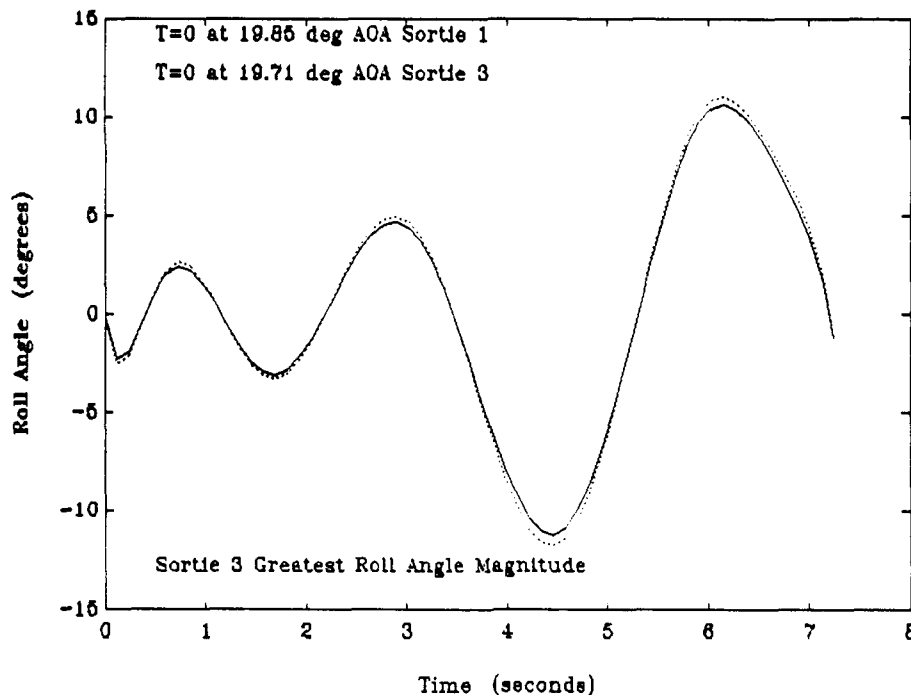


Figure 6.9. Roll Angle Magnitude Following Wing Rock Onset

Figure 6.8 shows the linear (disregarding DAS noise) growth of angle-of-attack while figure 6.9 shows an increasing roll angle magnitude for each cycle as  $\alpha$  is increased. Unlike the T-38A, the RF-4C roll oscillations are not symmetric about the roll axis. Each oscillation continues the growth in roll angle magnitude. Test data from flight three showed oscillations of greater magnitude but the frequency characteristics of the motion are essentially the same. The initial frequency is 1 complete cycle in 1.2 seconds or .83 cycles/sec. The frequency prediction parameter (equation 3.34) predicted a frequency of 1.3 cycles/sec. Thus wing rock onset for the RF-4C is much lower than predicted. Figure 6.10 illustrates the limit cycle mechanism of wing rock. For safety reasons the test maneuver was terminated before the full development of a limit cycle phenomenon could be seen.

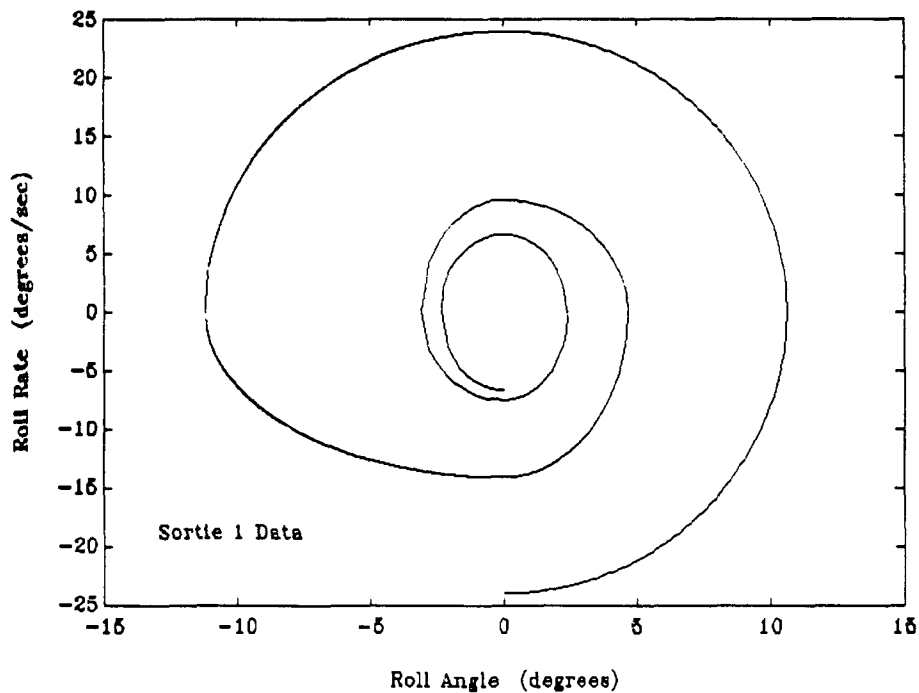


Figure 6.10. RF-4C Wing Rock Limit Cycle

The RF-4C wing rock motion begins in the center of figure 6.10. As opposed to the T-38A wing rock motion, the rolling motion for the RF-4C was not symmetric about the roll axis. For the RF-4C each rolling oscillation increased in magnitude as angle-of-attack was increased. The nature of this motion produced a circular spiral type of motion on the plot of roll angle versus roll rate. This motion appears to be approaching the limit cycle bounded by  $\pm 24^\circ/\text{sec}$  roll rate and  $\pm 11^\circ$  roll angle. As the RF-4C roll oscillations grew in magnitude the roll rate oscillations also grew until increased damping at higher roll angles resulted in the established roll oscillation limit. As stated earlier this mechanism was not fully illustrated by the RF-4C flight test phase due to the short time period this phenomenon was allowed to develop before aircraft recovery was required.

RF-4C Test Crew Comments. A single test pilot and two flight test weapon system

officers (WSO) participated in the RF-4C flight test phase. As with the T-38A qualitative comments were obtained through magnetic tape recordings of cockpit voice recorded during the practice test maneuver and the actual data run. Along with the recorded information, discussions with the test team members during the flight debriefs were also used to gain qualitative data concerning the onset of wing rock. The RF-4C test pilot commented that the onset of wing rock in the RF-4C was "like turning on a switch at 20° AOA". The pilot also stated that the roll oscillations were repeatable, relatively mild, with increasing magnitude and that he saw roughly the same things on each 1-G stall he performed. The test pilot also agreed that the flight test technique (RF-4C 1-G stall) was appropriate to collect the data required for this thesis.

Both test WSOs were specifically asked before the flights to attempt to observe the unstable motion occurring at wing rock onset and comment upon roll angle magnitude, pitch angle oscillations and sideslip changes. The test WSOs agreed that the wing rock motion appeared to be a relatively mild, with magnitude increasing, rolling motion with little or no pitch or yaw oscillations present. Recorded data supported these observations, the pitch data increased or decreased with AOA (within DAS noise levels) while the largest angle-of-sideslip recorded during the wing rock oscillations was .814°.

## VII. Conclusions and Recommendations

### Conclusions

1. Bifurcation analysis was a useful tool when used to investigate the highly nonlinear aircraft behavior of wing rock. This technique allows large portions of the aircraft flight envelope to be analyzed fairly accurately. This method predicted wing rock onset in the F-15B to within one degree of flight test data.

2. An application of small perturbation theory can be used to examine the onset of a large perturbation phenomenon if small angle assumptions are not made. In this case, small perturbation theory was used to linearize a highly nonlinear set of equations about a single point. This linearization led to the development of the trigger parameter derived in Chapter 3.

**The following conclusions are based on a fighter aircraft with a swept wing maneuvering near the 1-G stall.**

3. The rolling oscillations that are commonly referred to as wing rock are actually unstable dutch roll motions. These oscillations usually precede the stall and for some configurations are a good indicator of impending departure. An unstable dutch roll motion may consist of considerable roll and yaw at low angles-of-attack however, this motion becomes more of a pure rolling motion as  $\alpha$  is increased.

4. The trigger parameter and the simple procedure developed to predict wing rock are fairly accurate for a swept wing fighter design. Unlike LCDP or  $C_{n\beta, dynamic}$ , which

were developed to give a rough indication of unfavorable high AOA behavior, the trigger parameter ( $X_{\theta}$ ) will predict the actual wing rock onset AOA. The developed technique predicted wing rock onset for three different fighter aircraft (F-15B, RF-4J/C, and T-38A. Here the RF-4C and the F-4J will be considered one design) with three distinct planforms. The procedure appears to be accurate to within  $1^\circ$  and was verified with both wind tunnel and flight test data.

5. The frequency prediction parameter (equation 3.34) was found to be less accurate. This predictor was not able to accurately predict the first rapid roll oscillation which was characteristic of T-38A wing rock onset. The method was able to predict F-15B and F-4 initial motion frequency to within .5 cycles/sec. Wing rock motion was shown to grow at a fairly quick rate and this initial frequency may not be that critical. A more useful piece of information would be the frequency of the motion once the limit cycle of the behavior is reached. This parameter may be adversely affected by the method used to gather flight test data. Frequency data was not obtained at a trimmed flight condition.

6. The critical stability derivatives involved in the development of or at least in the prediction of wing rock are  $C_{l_p}$ , roll damping, and  $C_{l_\beta}$ , dihedral effect. The critical situation for wing rock development appears to be an increase in dihedral effect with a corresponding rapid decrease in roll damping as angle-of-attack is increased. These derivatives are mostly a function of the aircraft's wing. Airfoil type, wing placement, aspect ratio, sweepback and dihedral all have a large effect on the magnitude and sign of the critical stability derivatives. The very wing characteristics which lend themselves

to increased fighter performance also produce the undesirable handling quality of wing rock.

Complimenting the development of the triggering parameter, Roskam (23) has previously shown that a negative increase in  $C_{l\dot{\alpha}}$  results in a corresponding decrease in dutch roll damping. Roll damping and dihedral effect exist in a conflicting relationship. A fighter aircraft with a highly swept wing designed to produce large roll rates will have a large negative value of  $C_{l\dot{\alpha}}$  and a relatively small negative value of  $C_{l\beta}$  and the magnitude difference between these parameters will grow with an increase in angle-of-attack. An aircraft with these characteristics will have a greater tendency to exhibit wing rock behavior.

7. Along with the critical stability derivatives discussed in conclusion 6, another factor critical to the development and growth of wing rock is the distribution of mass about the aircraft's roll axis. Upon comparison of the RF-4C and the T-38A flight tests the obvious was revealed, the aircraft with the smallest distribution of mass about the body x-axis exhibited the greatest roll angle magnitudes and the quickest roll rates during wing rock.

It appears that the slope of the trigger parameter versus alpha curve gives an indication of the frequency and magnitude of the wing rock oscillations. The slope of this curve is heavily influenced by the distribution of mass about the aircraft x-axis. The F-4J, RF-4C and the F-15 are roughly the same weight and size and have similar mass distributions about their respective x-axes. These aircraft types produced trigger parameter plots with approximately the same slope. The T-38 however, with very little

mass distributed about the X-axis, displayed a much steeper trigger parameter curve and the wing rock oscillations of the Talon were larger and faster than either model of the F-4. With only two real examples (flight test data) further evidence is required to confirm this conclusion.

### Recommendations

This thesis only looked at wing rock in a very specific manner and is by no means a complete investigation. Therefore, the following recommendations for further study are made.

1. Recommend that further analysis be accomplished to expand the flight envelope within which the trigger parameter is useful. The analysis techniques used by this thesis could be applied to turning flight to produce a method to predict wing rock in or near the accelerated stall. This data would probably be more useful to the fighter aircraft designer as the accelerated stall is often approached in close-in combat during a tracking task. The analysis could also be expanded into the airspeed range of compressibility, again to provide further understanding of wing rock in a more realistic environment.

2. An attempt to predict the actual limit cycle of wing rock would provide the aircraft designer with the maximum roll rate and roll angle produced by this behavior. These numbers would probably be more useful than a frequency prediction parameter that predicts the initial rolling oscillation.

3. These techniques could also be applied to an aircraft with an unconventional wing

design (forward swept or oblique) and conclusions compared. Another interesting design to look at would be a lifting body design which exhibited wing rock behavior (an aircraft with little or no wing) to determine if the stability derivatives contributing to the development of wing rock remain the same.

3. With the advent of advanced computer aided flight control systems this phenomenon does not appear to be that critical. However, a good baseline design may eliminate many problems for the control systems engineers. Control schemes that increase  $X_\phi$  should be studied and if relevant employed to eliminate the undesirable characteristics of wing rock.

## Appendix A: F-15 Physical Data

The following data was taken from a McDonnell Douglas report on mass and inertia characteristics (12).

### Wing

area (theoretical)	608 Sq. Ft.
aspect ratio	3.01
Airfoil	
root	NACA64006.6
Xw 155	NACA64A(x)04.6(a=0.8 MOD)
tip	NACA64A203(a=0.8 MOD)
span	42.8 Ft.
taper ratio	.025
root chord	273.3 In.
tip chord	68.3 In.
mean aerodynamic chord	191.3 In.
leading edge sweep angle	45°
25% chord sweep angle	38.6°
dihedral	-1°
twist at tip	none
incidence	none
aileron area	26.5 Sq. Ft.
flap area	35.8 Sq. Ft.

### Speed Brake

area	31.5 Sq. Ft.
------	--------------

### Control Surface Movement

aileron	±20°
speedbrake	45° up
flap	30° down
horizontal tail	29° down, 15° up
rudder	±30°

### Vertical Tail

area	62.6 Sq. Ft.
rudder area (each)	10.0 Sq. Ft.
span	10.3 Ft.
aspect ratio	1.7
root chord	115 In.
tip chord	30.6 In.

airfoil - root	NACA0005-64
tip	NACA0003.5-64
taper ratio	0.27
leading edge sweep angle	36.6°
25 % chord sweep angle	29.7°
mean aerodynamic chord	81 In.
cant	2° out
length	212.4 In.

#### Horizontal Tail

area	111.4 Sq. Ft.
span	15.7 Ft.
aspect ratio	2.05
taper ratio	0.34
root chord	137.2 In.
tip chord	46.5 In.
airfoil - root	NACA0005.5-64
tip	NACA0002.5-64
leading edge sweep angle	50°
25 % chord sweep angle	43.6°
mean aerodynamic chord	99.3 In.
dihedral	.0°
length	241 In.

#### Wetted Area (Sq. Ft.)

fuselage	1405
nozzles	.53
horizontal tail	216
vertical tail	257
wing	698
total	2629

#### Fuel Capacity

fuselage	.944 gal
wing	.846 gal
three external tanks	1830 gal

#### Miscellaneous Data

aircraft length	63.8 Ft.
aircraft height	18.6 Ft.
aircraft volume	1996 cubic Ft.

The following inertia data is based on a clean aircraft carrying 50% fuel, a full load of

20mm gun ammunition and 4 aim-7F missiles.

$$I_x = 25480 \text{ slug-ft}^2$$

$$I_y = 166620 \text{ slug-ft}^2$$

$$I_z = 186930 \text{ slug-ft}^2$$

$$I_{xz} = -1000 \text{ slug-ft}^2$$

## Appendix B: F-4 Physical Data

### Wing

area	530 Sq. Ft.
span	38.67 Ft.
aspect ratio	2.82
mean aerodynamic chord	16.04 Ft.

### Aircraft

height	16 Ft. 5 In.
length	63 Ft.
fuel weight	6000 LBS.
total weight	41000 LBS.

### Control Surface Deflections

horizontal tail	+ 9°, -21°
ailerons	30° down
spoilers	43° up
rudder	± 30°

The following inertia data is for a cruise configuration (clean aircraft) with 50% internal fuel.

$$I_x = 23,850 \text{ slug-ft}^2$$

$$I_y = 127,400 \text{ slug-ft}^2$$

$$I_z = 146,000 \text{ slug-ft}^2$$

$$I_{xz} = 1210 \text{ slug-ft}^2$$

## Appendix C: T-38 Physical Data

### Wing

area	170 Sq. Ft.
span	25 Ft. 3 In.
aspect ratio	3.75
tapper ratio	0.2
sweepback	24°
airfoil	NACA65A004.8 (MOD)
mean aerodynamic chord	92.76 In.
dihedral	none
incidence	none
span/thickness	51.1

### Horizontal Tail

area	33.34 Sq. Ft.
aspect ratio	2.82
taper ratio	0.33
sweepback	25°
airfoil section	NACA65A004
span/thickness	58.6

### Vertical Tail

area	41.07 Sq. Ft.
aspect ratio	1.21
taper ratio	0.25
sweepback	25°
airfoil section	NACA65A004 (MOD)
span/thickness	42.2

### Aircraft

height	12 Ft. 11 In.
length	43 Ft. 1 In.
fuel weight	3880 LBS
total weight	11,250 LBS

### Control Surface Deflections

horizontal tail	+8° -17°
ailerons	
gear down	+25° -35°
gear up	+14° -18.5°

rudder	
gear down . . . . .	$\pm 30^\circ$
gear up . . . . .	$\pm 6^\circ$
flaps	
takeoff . . . . .	$20^\circ$
landing . . . . .	$45^\circ$

The following inertia data is for a clean aircraft carrying 50% fuel.

$$\begin{aligned}
 I_x &= 1479 \text{ slug-ft}^2 \\
 I_y &= 24,000 \text{ slug-ft}^2 \\
 I_z &= 29,047 \text{ slug-ft}^2 \\
 I_{xz} &= -80 \text{ slug-ft}^2
 \end{aligned}$$

## Appendix D: Fighter Inertia Characteristics

Aircraft	$I_x$	$I_y$	$I_z$	$I_{xz}$	$\frac{I_{xz}^2}{I_x I_z}$	$\frac{I_{xz}}{I_x}$
F-4J	23850	127400	146000	1210	.0004	.05
F-15B	25480	166620	186930	-1000	.0002	-.03
F-16B	7675	48640	54260	-290	.0002	-.03
T-38A	1479	24000	29047	-80	.00015	-.05

all inertia values presented in slugs feet squared

## Appendix E: DAS Parameter Listings

RF-4C

Primary TM Frequency: 1444.5

PARAMETER	UNITS	RANGE MIN	RANGE MAX	ACCURACY	AYDIN- VECTOR RESOLUTION UNITS
Rt Engine Fuel Flow	Gal/Min	0	22	0.2	0.0859
Rt AB Fuel Flow	Gal/Min	0	65	0.5	0.2539
Rt Fuel Used	Gal	0	2000	0.1	0.0305
Lt Engine Fuel Flow	Gal/Min	0	22	0.2	0.0859
Lt AB Fuel Flow	Gal/Min	0	65	0.5	0.2539
Lt Fuel Used	Gal	0	2000	0.1	0.0305
Event Counter	Count	0	99		
Run Counter	Count	0	99		
Event Marker	On/Off	0	255		
Pitch Angle	Degress	-90	90	1.0	0.7031
Roll Angle	Degress	-180	180	2.0	1.4063
Longitudinal Stick Force	Lbs	-40	40	1.0	0.3125
Lateral Stick Force	Lbs	-20	20	0.7	0.1563
Rudder Pedal Force	Lbs	-180	180	3.0	1.4063
Pitch Rate	Deg/Sec	-20	20	2.0	0.1563
Roll Rate	Deg/Sec	-360	360	2.0	0.7031
Yaw Rate	Deg/Sec	-20	20	2.0	0.1563
Indicated Airspeed	Knots	0	850	0.9	0.0130
Altitude	Feet	0	50000	5.0	0.7629
Right Engine RPM	% RPM	40	110	0.5	0.2734
Left Engine RPM	% RPM	40	110	0.5	0.2734
Angle of Attack	Degrees	-35	35	0.5	0.2734
Angle of Sideslip	Degrees	-25	25	0.5	0.1953
Rt Engine Fuel Temp	Deg C	-50	150	2.0	0.7813

Lt Engine Fuel Temp	Deg C	-50	150	2.0	0.7813
Outside Air Temp	Deg C	-55	85	1.5	0.5469
Normal Acceleration	G	-3	8	0.1	0.0430
Longitudinal Acceleration	G	-1	1	0.1	0.0078
Lateral Acceleration	G	-1	1	0.1	0.0078
Longitudinal Stick Position	Inches	0	6	0.2	0.0234
Lateral Stick Position	Inches	-4	4	0.2	0.0313
Rudder Pedal Position	Inches	-4	4	0.2	0.0313
Stabulator Position	Degrees	-8	20	1.0	0.1094
Rt Aileron Position	Degrees	-30	0	1.0	0.1172
Lt Aileron Position	Degrees	-30	0	1.0	0.1172
Rudder Position	Degrees	-30	30	1.0	0.2344
Rt Spoiler Position	Degrees	0	45	1.0	0.1758
Lt Spoiler Position	Degrees	0	45	1.0	0.1758
Time					
Hot Mike					

Primary TM Frequency: 1448.5

PARAMETER	UNITS	RANGE MIN	RANGE MAX	ACCURACY	METROPLEX RESOLUTION (UNITS)
Rt Engine Fuel Flow	Gal/Min	0	22	0.2	0.0215
Rt AB Fuel Flow	Gal/Min	0	65	0.5	0.0635
Rt Fuel Used	Gal	0	2000	0.1	0.0019
Lt Engine Fuel Flow	Gal/Min	0	22	0.2	0.0215
Lt AB Fuel Flow	Gal/Min	0	65	0.5	0.0635
Lt Fuel Used	Gal	0	2000	0.1	0.0019
Event Counter	Count	0	99		
Run Counter	Count	0	99		
Event Marker	On/Off	0	255		
Pitch Angle	Degress	-90	90	1.0	0.1758
Roll Angle	Degress	-180	180	2.0	1.3516
Longitudinal Stick Force	Lbs	-40	40	1.0	0.0781
Lateral Stick Force	Lbs	-20	20	0.7	0.0391
Rudder Pedal Force	Lbs	-180	180	3.0	0.3516
Pitch Rate	Deg/Sec	-20	20	2.0	0.0391
Roll Rate	Deg/Sec	-360	360	2.0	0.7031
Yaw Rate	Deg/Sec	-20	20	2.0	0.0391
Indicated Airspeed	Knots	0	850	0.9	0.0008
Altitude	Feet	0	50000	5.0	0.0477
Right Engine RPM	% RPM	40	110	0.5	0.0684
Left Engine RPM	% RPM	40	110	0.5	0.0684
Angle of Attack	Degrees	-35	35	0.5	0.0684
Angle of Sideslip	Degrees	-25	25	0.5	0.0488
Rt Engine Fuel Temp	Deg C	-50	150	2.0	0.1953
Lt Engine Fuel Temp	Deg C	-50	150	2.0	0.1953

Outside Air Temp	Deg C	-55	85	1.5	0.1367
Normal Acceleration	G	-3	8	0.1	0.0107
Longitudinal Acceleration	G	-1	1	0.1	0.0020
Lateral Acceleration	G	-1	1	0.1	0.0020
Longitudinal Stick Position	Inches	0	6	0.2	0.0059
Lateral Stick Position	Inches	-4	4	0.2	0.0078
Rudder Pedal Position	Inches	-4	4	0.2	0.0078
Stabilitator Position	Degrees	-8	20	1.0	0.0273
Rt Aileron Position	Degrees	-30	0	1.0	0.0293
Lt Aileron Position	Degrees	-30	0	1.0	0.0293
Rudder Position	Degrees	-30	30	1.0	0.0586
Time					
Hot Mike					

### Bibliography

1. Air Force Flight Test Center. *F-15A Approach-to-Stall/Stall/Post Stall Evaluation*. AFFTC-TR-75-32. Edwards AFB CA: HQ AFFTC, January 1976 (AD-B045115).
2. Arena, A.S. and R. C. Nelson. "An Experimental Study of the Nonlinear Dynamic Phenomenon Known as Wing Rock," *AIAA Atmospheric Flight Mechanics Conference*. Paper No 88-4371-CP. Washington, D.C.: American Institute of Aeronautics and Astronautics, August 1988.
3. Barth, Capt Thomas J. *Determination of High Angle-of-Attack Stability of the F-15B Aircraft Using Bifurcation Analysis*. MS Thesis, AFIT/GAE/AA/87D-1. School of Engineering, Air Force Institute of Technology (AU), Wright-Patterson AFB OH, December 1987.
4. Beck, Capt J. A. *Bifurcation Analysis of a Model Fighter Aircraft with Control Augmentation*. Ms Thesis, AFIT/GAE/ENY/89D-02. School of Engineering, Air Force Institute of Technology (AU), Wright-Patterson AFB, December 1989.
5. Carroll, James V. and R. K. Mehra. "Bifurcation Analysis of Nonlinear Aircraft Dynamics," AIAA paper 82-4254, *Journal of Guidance and Control*, 5: 529-536 (September-October 1982).
6. Doedel, E.J. and J.P. Kervenez. "Software for Continuation Problems in Ordinary Differential Equations with Applications." Preprint, Pasadena, CA: California Institute of Technology, 1984.
7. Ericsson L.E. "Slender Wing Rock Revisited," *AIAA Atmospheric Flight Mechanics Conference*. Paper No 91-0417. Washington, D.C. : American Institute of Aeronautics and Astronautics, January 1991.
8. Fromme, W.M. et al. *T-38 Static Stability and Basic Aerodynamic Data*. NAI-58-578. Northrop Aircraft, Inc. Hawthorne, CA, October 1958.
9. Hwang, C. and W.S. Pi. "Some Observations on the Mechanism of Aircraft Wing Rock," *Journal of Aircraft*, 16: 366-373 (June 1979).
10. Hsu, C.H. and C.E. Lan. "Theory of Wing Rock," *Journal of Aircraft*, 22: 920-924 (October 1985).

11. Johnston, D.E. *et al.* *Investigation of High-Angle-of-Attack Maneuver-limiting Factors*. Technical Report AFWAL-TR-80-3141. Wright-Patterson AFB OH: AFWAL, December 1980.
12. Lang, J.D. *Aircraft Performance, Stability and Control*. Aero 356 Course Notes. USAF Academy, USAFA, Co, August 1971.
13. Liff, K.W. "Subsonic Stability and Control Derivatives for an Unpowered, Remotely Piloted 3/8 Scale F-15," NASA N76-15176, 1976.
14. McDonnell Aircraft Company. *F-15 Flight Control System Description*. Design note DN1180.01-238-458 (Rev D), October 1981.
15. McDonnell Aircraft Company. *F-15 Stability Derivatives, Mass and Inertia Characteristics, Part I*. Report No MDC A4172, contract no F33657-70-0300, 1 August 1976.
16. McRuer, Duane *et al.* *Aircraft Dynamics and Automatic Control*. Princeton NJ: Princeton University Press, 1973.
17. Nelson, Robert C. *Flight Stability and Automatic Flight Controls*. New York: McGraw-Hill, 1989.
18. Nguyen L.T. and W.P. Gilbert. "Application of High- $\alpha$  Control System Concepts to a Variable-Sweep Fighter Airplane," NASA Langley Research Center, Hampton, Virginia. 1979.
19. Nguyen, L.T. *et al.* *Control-System Techniques for Improved Departure/Spin Resistance for Fighter Aircraft*. NASA Technical Report # 1689. Langley Research Center, Hampton, Virginia. 1980.
20. Nguyen, L.T. and A.J. Ross. "Some Observations Regarding Wing Rock Oscillations at High Angles of Attack," *AIAA Atmospheric Flight Mechanics Conference*. Paper No 88-4371-CP. Washington, D.C.: American Institute of Aeronautics and Astronautics, August 1988.
21. Planeaux, J.B. and T.J. Barth. "High-Angle-of-Attack Dynamic Behavior of a Model High-Performance Fighter Aircraft," *AIAA Atmospheric Flight Mechanics Conference*. Paper No 88-4368. Washington, D.C.: American Institute of Aeronautics and Astronautics, August 1988.

22. Planeaux, J.B. and J.A. Beck. "Bifurcation Analysis of a Model Fighter Aircraft with Control Augmentation," *AIAA Atmospheric Flight Mechanics Conference*. Paper No 89-4753. Washington, D.C.: American Institute of Aeronautics and Astronautics, August 1989.
23. Roskam, J. *Airplane Flight Dynamics and Automatic Flight Controls*. Lawrence, Kansas: Roskam Aviation and Engineering Corporation, 1979.
24. Ross, A.J. "Lateral Stability at High Angles of Attack, Particularly Wing Rock," *Controller HMSO*, London, 1978.
25. Schmidt, L.V. "Wing Rock due to Aerodynamic Hysteresis," *Journal of Aircraft*, 16: 129-133 (March 1979).
26. Seydel, R. *From Equilibrium to Chaos: Practical Bifurcation and Stability Analysis*. New York: Elsevier Press, 1988.
27. Smith, B.T. *Matrix Eigensystem Routines, EISPACK Guide 2nd Edition*, 1974.
28. Strang, G. *Linear Algebra and Its Applications*. San Diego, California: Harcourt Brace Jovanovich, 1988.
29. *USAF Series Aircraft, RF-4C Flight Manual*, Technical Order 1RF-4C-1, 15 October 1984. Aircraft Partial RF-4C 65-850.
30. *USAF Series Aircraft, F-15A/B/C/D Flight Manual*, Technical Order 1F-15A-1, 1 July 1989, Change 3, 15 January 1991.
31. *USAF Series Aircraft, T-38A/B Flight Manual*, Technical Order 1T-38A-1, 1 July 1987, Change 3, 1 May 1990.
32. Waltman, P. *A Second Course In Elementary Differential Equations*. Orlando, Florida: Academic Press, 1986.
33. Zagaynov, G.I. and M.G. Goman. "Bifurcation Analysis of Critical Aircraft Flight Regimes," *International Council of the Aeronautical Sciences*, 84: 217-223, 1984.

## VITA

Capt Robert C. Nolan was born on 9 May 1961 in Everett, Massachusetts. He graduated from high school in Ithaca, New York, in 1979. He then attended the United States Air Force Academy, receiving a Bachelor of Science Degree in Aeronautical Engineering in June 1983. After receiving his commission in the USAF in June, 1983, he entered undergraduate pilot training at Williams AFB, Arizona. Capt Nolan graduated from pilot training in July, 1984 and was assigned to the 334th Tactical Fighter Squadron, 4th Tactical Fighter Wing, Seymour-Johnson AFB, North Carolina as an F-4E pilot. While an F-4E pilot he served as a Wing Nuclear Weapons Instructor and became the Air Force's first operational crew member to successfully employ the IR GBU-15 Glide Bomb. Capt Nolan was named the 4th Tactical Fighter Wing Top Gun for the second half of 1987. Following his first assignment, Capt Nolan was assigned to the 85th Flying Training Squadron, Laughlin AFB, Texas, as a T-37 Instructor. While assigned to Laughlin, he served as the C-Flight Commander, 47 Flying Training Wing Evaluation Pilot, and Wing Spin Pilot. In July, 1990, Capt Nolan entered the joint AFIT/TPS program.

Permanent Address: 3 Lowell Place  
Ithaca, New York 14850

# REPORT DOCUMENTATION PAGE

Form Approved  
OMB No. 0704-0188

Public reporting burden for this collection of information is estimated to average 1 hour per response, including the time for reviewing instructions, searching existing data sources, gathering and maintaining the data needed, and completing and reviewing the collection of information. Send comments regarding this burden estimate or any other aspect of this collection of information, including suggestions for reducing this burden, to Washington Headquarters Services, Directorate for Information Operations and Reports, 1215 Jefferson Davis Highway, Suite 1204, Arlington, VA 22202-4302, and to the Office of Management and Budget, Paperwork Reduction Project (0704-0188), Washington, DC 20503.

1. AGENCY USE ONLY (Leave blank)

2. REPORT DATE

May 1992

3. REPORT TYPE AND DATES COVERED

Masters Thesis

4. TITLE AND SUBTITLE

Wing Rock Prediction Method for a High Performance Fighter Aircraft

5. FUNDING NUMBERS

6. AUTHOR(S)

Robert C. Nolan II, Capt, USAF

7. PERFORMING ORGANIZATION NAME(S) AND ADDRESS(ES)

AFIT (AU)  
Wright-Patterson AFB, OH 45324

8. PERFORMING ORGANIZATION  
REPORT NUMBER

AFIT/GAE/ENY/92J-02

9. SPONSORING / MONITORING AGENCY NAME(S) AND ADDRESS(ES)

USAFTPS  
Edwards AFB, CA 93523

10. SPONSORING / MONITORING  
AGENCY REPORT NUMBER

11. SUPPLEMENTARY NOTES

Prepared as part of the joint AFIT/TPS program.

12a. DISTRIBUTION / AVAILABILITY STATEMENT

Unlimited

12b. DISTRIBUTION CODE

13. ABSTRACT (Maximum 200 words)

This study is a limited investigation of the non-linear aircraft behavior known as wing rock. An eight state F-15 model is analyzed using bifurcation theory. The wing rock onset point is identified and small perturbation analysis is used to linearize the equations of motion about this point. The eigenstructure of the model is analyzed and is used to identify the stability modes involved in this motion. A procedure is developed to predict wing rock onset and frequency and the critical stability derivatives involved in this motion are identified. The developed procedure is applied to existing F-4J data and a flight test involving RF-4C and T-38A aircraft is flown. The results show wing rock is an unstable dutch roll motion and the developed wing rock prediction parameter is accurate to within 1 degree of onset AOA. The frequency prediction parameter gives a fair estimate of wing rock motion but it may be adversely influenced by the type of flight test data. The slope of the prediction parameter versus AOA curve may be an indication of the severity of wing rock motion.

14. SUBJECT TERMS

Stability and control, bifurcation (mathematics), wing rock, roll oscillations, flight test, high AOA.

15. NUMBER OF PAGES

124

16. PRICE CODE

17. SECURITY CLASSIFICATION  
OF REPORT

unclassified

18. SECURITY CLASSIFICATION  
OF THIS PAGE

unclassified

19. SECURITY CLASSIFICATION  
OF ABSTRACT

unclassified

20. LIMITATION OF ABSTRACT

UL